

# Analysis of the functional consequences of p97 mutations leading to the multisystem disorder IBMPFD

INAUGURAL-DISSERTATION  
zur  
Erlangung des Doktorgrades  
der Mathematisch-Naturwissenschaftlichen Fakultät  
der Universität zu Köln



vorgelegt von

Christian Ulrich Hübbers

aus Köln

Druck: Copy-Star GmbH Köln

2007



Referees/Berichterstatter:

Prof. Dr. Angelika A. Noegel  
Prof. Dr. Thomas Langer

Date of oral examination:  
(Tag der mündlichen Prüfung)

21.11.2007

The present research work was carried out under the supervision of Prof. Dr. Angelika A. Noegel and Dr. Christoph S. Clemen, in the Institute of Biochemistry I, Medical Faculty, University of Cologne (Cologne, Germany) from November 2004 to November 2007.

Diese Arbeit wurde von November 2004 bis November 2007 am Biochemischen Institut I der Medizinischen Fakultät der Universität zu Köln unter der Leitung von Prof. Dr. Angelika A. Noegel und Dr. Christoph S. Clemen durchgeführt.



# Contents

<b>1.</b>	<b>ACKNOWLEDGEMENT.....</b>	<b>7</b>
<b>2.</b>	<b>INTRODUCTION.....</b>	<b>9</b>
2.1.	FUNCTIONAL ROLE OF P97 AND ITS COFACTORS .....	9
2.2.	FUNCTION OF P97 IN THE ERAD PATHWAY .....	11
2.3.	THE ALTERNATIVE DEGRADATION SYSTEM AUTOPHAGY IS FUNCTIONALLY COUPLED TO THE UPS .....	12
2.4.	CHARACTERIZATION OF THE DISEASE IBMPFD .....	13
2.5.	CLINICAL OBSERVATIONS IN PATIENTS INVOLVED IN THIS STUDY .....	14
2.6.	SCIENTIFIC QUESTIONS AND WORKING PLAN .....	17
<b>3.</b>	<b>RESULTS .....</b>	<b>18</b>
3.1.	MORPHOLOGICAL, ULTRASTRUCTURAL AND BIOCHEMICAL ANALYSIS OF THE SKELETAL MUSCLE AND CARDIAC PATHOLOGY .....	18
3.1.1.	<i>Skeletal muscle pathology.....</i>	<i>18</i>
3.1.2.	<i>Cardiac pathology .....</i>	<i>22</i>
3.1.3.	<i>p97 protein expression in IBMPFD muscle.....</i>	<i>22</i>
3.1.4.	<i>Analysis of normal and IBMPFD primary human myoblasts .....</i>	<i>24</i>
3.2.	GENERATION AND CHARACTERIZATION OF WT AND MUTANT P97 CONSTRUCTS .....	26
3.2.1.	<i>Immunofluorescence analysis of p97 overexpressing cells .....</i>	<i>27</i>
3.2.2.	<i>1D- and 2D SDS-PAGE followed by immunoblotting of p97 overexpressing cells and primary myoblasts .....</i>	<i>33</i>
3.2.3.	<i>Cell proliferation assay.....</i>	<i>36</i>
3.3.	P97 RESPONSE TO CELLULAR STRESS .....	37
3.3.1.	<i>Use of various cell stressors to induce p97 aggregates .....</i>	<i>37</i>
3.3.2.	<i>Time course of aggregate formation and clearance .....</i>	<i>38</i>
3.4.	STUDY OF PROTEASOME AND ERAD ACTIVITIES .....	40
3.4.1.	<i>Proteasomal activity .....</i>	<i>40</i>
3.4.2.	<i>Defects in ERAD activity in the presence of mutated p97.....</i>	<i>42</i>
3.4.3.	<i>Fluorescence protease protection assay analysis of ER and Golgi morphology.....</i>	<i>46</i>
3.4.4.	<i>Fluorescence protease protection assay of autophagosomes .....</i>	<i>51</i>
3.5.	FILTER ASSAY COMBINED WITH GC/MS ANALYSIS OF PUTATIVE LIGANDS BINDING TO RECOMBINANT P97 .....	54
3.6.	GENERATION OF A R155C-P97 MOUSE KNOCK-IN TARGETING VECTOR .....	55
<b>4.</b>	<b>DISCUSSION .....</b>	<b>58</b>
4.1.	CLINICAL PHENOTYPE.....	58
4.2.	ANALYSIS OF THE P97 PROTEIN EXPRESSION AND LOCALIZATION.....	59
4.3.	STRUCTURAL ANALYSIS OF WILD TYPE P97 VERSUS R93 AND R155 MUTANT P97 .....	60
4.3.1.	<i>In silico screening of small ligand binding .....</i>	<i>64</i>
4.4.	ANALYSIS OF PROTEASOME AND ERAD ACTIVITY .....	66
4.5.	ROLE OF P97 IN THE REGULATORY ERAD PATHWAY .....	67
4.6.	OUTLOOK .....	68

<b>5.</b>	<b>MATERIALS AND METHODS .....</b>	<b>70</b>
5.1.	MAMMALIAN CELL CULTURE.....	70
5.1.1.	<i>Culture conditions</i> .....	70
5.1.2.	<i>Transfection methods</i> .....	71
5.1.3.	<i>Generation of growth curves</i> .....	72
5.1.4.	<i>Cell stress experiments</i> .....	72
5.2.	IMAGING.....	73
5.2.1.	<i>Indirect immunofluorescence and imaging of living cells</i> .....	73
5.2.2.	<i>Fluorescence protein protection (FPP) assay</i> .....	74
5.3.	GEL ELECTROPHORESIS AND WESTERN BLOTTING.....	75
5.4.	P97-CDNA, SITE-DIRECTED MUTAGENESIS AND PLASMIDS: .....	76
5.5.	GENERATION OF MOUSE TARGETING VECTOR .....	77
5.6.	HISTOLOGICAL ANALYSIS .....	78
5.7.	ANTIBODIES.....	78
5.8.	PROTEIN PURIFICATION.....	80
5.9.	FILTER ASSAY.....	81
5.10.	PROTEASOME ASSAY .....	81
5.11.	STATISTICAL ANALYSIS .....	83
<b>6.</b>	<b>REFERENCES.....</b>	<b>84</b>
<b>7.</b>	<b>ABBREVIATIONS .....</b>	<b>98</b>
<b>8.</b>	<b>ABSTRACT .....</b>	<b>99</b>
<b>9.</b>	<b>ZUSAMMENFASSUNG .....</b>	<b>100</b>
<b>10.</b>	<b>ERKLÄRUNG.....</b>	<b>101</b>
<b>11.</b>	<b>CURRICULUM VITAE / LEBENSLAUF .....</b>	<b>102</b>

## **1. Acknowledgement**

This work would never have been accomplished without the helpfulness, willingness to share knowledge and support of many people.

I would like to thank them:

At first I have to thank my supervisor Dr. Christoph Clemen for his guidance throughout the course of this investigation and for always having an open eye and ear when discussing my work and writings.

I am deeply grateful to Prof. Angelika A. Noegel for offering me the opportunity to perform my PhD work in her lab and for all the thoughts and helpful suggestions.

I also owe my thanks to Prof. Rolf Schröder for supporting and discussing my work.

I thank Prof. Andreas Hofmann (Brisbane, Australia), Dr. Anett Böddrich (Berlin) and Prof. Franz-Georg Hanisch (Cologne) for collaboration.

My special thanks also go to Maria who always gave me excellent technical support and introduced me to the established methods in this lab.

I thank Berthold for fire fighting and for the help in all cell culture matters.

I have to thank Budi and Gudrun for giving me plenty of rope in all computer matters, Dörte for her help in administration issues, Bärbel, Brigitte and Sonja for preparing all this little common things that made laboratory work so easy and effective, and Martina, Rolf and Rosi for technical support in special issues.

Thanks also to the present and former members of Lab 12: André, Charles-Peter, Karthik, Markus, Raphael, Soraya and Vasily. Laboratory work was never boring with you.

All the present and former people I spent my time during the work in this institute, Eva-Maria, Jessica, Georgia, Carola, Marion, Francisco, Wenshu, Ria, Yvonne, Verena, Hafida, Sascha, Åsa, Akis, Hua, Mary, Subhanjan, Anne, Tanja, Deen, Vivek, Surayya, Rashmi, Jianbo, Rui, Marcel, Ludwig, Monika, Julia, Kristina, Claudia, Anke, Kira, Andrea, Maarten, Thomas, Dominic and Prof. Stefan Höning. Thank you for discussing my work, all the birthday cakes and other things in everyday's live that made my time interesting in scientific and personal matters.

.  
My parents I have to thank for all the support during my studies and in all other circumstances!

Steffi, I thank you for all the power and support. Your love means everything to me!

Christian

## 2. Introduction

### 2.1. Functional role of p97 and its cofactors

Mammalian p97 is an ubiquitously expressed member of the type II AAA (ATPase associated with various activities) ATPase family. Highly conserved orthologs are e.g. expressed in the archaebacterium *Sulfolobus acidocaldarius* (SAV), *Saccharomyces cerevisiae* (CDC48), *Dictyostelium discoideum* (cdcD), *Arabidopsis thaliana* (AtCDC48), and *Drosophila melanogaster* (TER94) thus demonstrating that p97 is an essential and evolutionary highly conserved cellular protein (Moir et al., 1982; Feiler et al., 1995; Confalonieri, et al. 1994; Pinter et al., 1998; Bakthavatsalam et al., 2007). The unfavourable name VCP (for valosin containing protein) was initially given to p97 after trying to purify the hormone peptide valosin but turned out to be an artefact (Koller and Brownstein, Nature 1987). p97 has a tripartite structure comprising an N-terminal domain (CDC 48) involved in ubiquitin binding, and two central D1- and D2-domains, which provide ATP binding and hydrolysis (DeLaBarre and Brünger, 2003). p97 assembles into functional hexamers with a central cylinder formed by the D-domains surrounded by the N-domains. The D1-domain is mainly responsible for p97 hexamerization while the D2-domain provides the major ATPase activity to p97 that enables it to function as a molecular chaperone interacting with a diverse group of adaptors to perform specific cellular functions (Zhang et al., 2000).

p97 has been associated with a wide variety of essential cellular processes comprising nuclear envelope reconstruction, the cell cycle, postmitotic Golgi reassembly, suppression of apoptosis, DNA damage response, the ubiquitin

proteasome protein degradation system and the endoplasmic reticulum associated protein degradation (ERAD) pathway (Kondo et al., 1997; Rabouille et al., 1998; Meyer et al., 2000; Hetzer et al., 2001; Ye et al., 2001; Rabinovich et al., 2002; Ye et al., 2004; Lilley and Ploegh, 2005).

Most, if not all of these functions seem to be directly linked to p97's ability to bind (multi-)ubiquitinated proteins and to segregate them from their binding partners, or to extract them from protein complexes (Rape et al., 2001; Meyer et al., 2002). The association of p97 with substrates is still not fully understood (Jentsch and Rumpf, 2007). *In vitro* binding studies indicate a direct interaction of ubiquitinated substrates with the N-domain of p97 (Dai and Li, 2001; Rape et al., 2001). However, the more common mechanism seems to be the indirect binding of p97's N-terminal domain to ubiquitinated substrates mediated by cofactors (Rape et al., 2001; Meyer et al. 2002; Hartmann-Petersen et al., 2004; Schubert et al., 2004; Richly et al., 2005).

Apart from these 'segregase' functions, p97 seems to influence the degree of ubiquitination of the bound substrates (Hartmann-Petersen et al., 2004; Richly et al., 2005). Hence, so-called 'substrate-processing cofactors' together with p97 can either promote polyubiquitination, inhibit polyubiquitination or deubiquitinate (multi-)ubiquitinated substrates (Koegl et al., 1999; Uchiyama et al., 2002; Burnett et al., 2003; Wang et al., 2004; Richly et al., 2005; Rumpf and Jentsch, 2006).

## 2.2. Function of p97 in the ERAD pathway

The ubiquitin-proteasome system (UPS) is a major degradation system for short-lived proteins (Hershko and Ciechanover, 1998). Proteins to be degraded are labeled with ubiquitin. Ubiquitin is conjugated through its carboxy terminus usually to  $\epsilon$ -amino groups of lysine residues. This conjugation typically involves three types of enzyme: E1 (ubiquitin-activating enzyme) hydrolyses ATP and forms a thioester-linked conjugate between itself and ubiquitin; E2 (ubiquitin-conjugating enzyme) receives ubiquitin from E1 and forms a similar thioester intermediate with ubiquitin; and E3 (ubiquitin ligase) binds both E2 and the substrate, and transfers the ubiquitin to the substrate. The ubiquitin itself can form a substrate for further rounds of ubiquitination, resulting in the formation of a polyubiquitin chain. Chains of four or more ubiquitin molecules (linked by lysines at residue 48) appear to form a recognition signal that allows substrates to be degraded by the 26S proteasome complex (Richly et al., 2005; Rubinsztein, 2006). The degradation is thus specifically targeted to selected proteins. Prompt removal of these proteins is critical to the precise and timely regulation of intracellular signaling involved in multiple cellular processes.

The endoplasmic reticulum-associated degradation (ERAD) pathway degrades initially endoplasmic reticulum (ER) localized protein substrates through the ubiquitin-proteasome system (Bonifacino and Weissman, 1998; Hampton, 2002). The ER is an intracellular membranous structure that performs such important functions as protein post-translational modifications, protein folding and oligomerization, and synthesis of lipids and sterols (Ding et al., 2007). Degradation prone proteins are abnormal (e.g. misfolded or misassembled) ER luminal and

membrane proteins as well as normal ER-resistant proteins for regulatory purposes. As the ubiquitin-proteasome system is absent from the ER lumen, these proteins have to be retrotranslocated to the cytosol or extracted from the ER membrane. p97 together with the cofactors Ufd1 and Npl4 is required for most ERAD substrates in an unclear mechanism which retrotranslocates or extracts or segregates them from a proposed retrotranslocation channel (Bays et al., 2001; Ye et al., 2001; Jarosch et al., 2002; Rabinovich et al., 2002; Braun et al., 2002; Elkabetz et al., 2004). Further general and/or specialized components like Ufd2, the homologues Rad23/Dsk2 and Ubx2 are involved in ERAD function (Medicherla et al., 2004; Schuberth et al., 2004; Richly et al., 2005)

### **2.3. The alternative degradation system autophagy is functionally coupled to the UPS**

Macroautophagy (referred as autophagy hereafter) is the second major intracellular degradation system. Unlike the UPS, autophagy is mainly responsible for the degradation of long-lived proteins and other cellular contents (Levine and Klionsky, 2004; Lum et al., 2005). Autophagy starts with the formation of double-membrane-bounded structures known as autophagosomes, or autophagic vacuoles (AVs). These fuse with lysosomes to form autophagolysosomes, and their contents are then degraded by acidic lysosomal hydrolases (Ravikumar and Rubinsztein, 2006).

Although the proteins targeted by autophagy and the UPS are different, the two systems serve a similar purpose in degrading proteins and recycling amino acids. Current studies demonstrated that the two cellular degradation systems are

functionally coupled and suppression of UPS activates autophagy (Brodsky and Scott, 2007; Ding et al., 2007; Pandey et al., 2007).

## 2.4. Characterization of the disease IBMPFD

Autosomal dominant inclusion body myopathy (IBM) associated with Paget disease of the bone (PDB) and frontotemporal dementia (FTD), or IBMPFD (OMIM 605382), is a late-onset human multisystem disorder caused by mutations of the p97 protein on chromosome 9p13-p12 (Watts et al., 2004; Haubenberger et al., 2005; Schröder et al., 2005). Apart from R191Q and A232E mutations, which reside in the N-D1-linker region and D1-domain, respectively, all other pathogenic mutations described so far are located in exons coding for the CDC48 domain of the p97 protein (Watts et al., 2004; Haubenberger et al., 2005; Schröder et al., 2005).

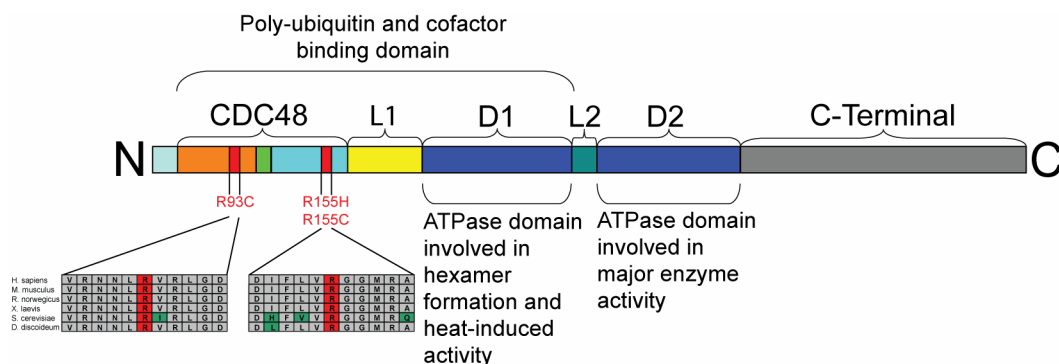


**Fig. 1. Domain structure of the p97 protein:**

CDC48 domain composed of double  $\psi$  barrel (amino acids 25–106, orange) and the four-stranded  $\beta$  barrel (amino acids 112–186, cyan), connected by a short linker region (amino acids 107–111, green). The CDC48 domain connects the D1-AAA-ATPase domain (amino acids 208–459, blue) by a linker region (amino acids 187–208, yellow). Linker region L2 (dark green), second AAA-ATPase domain (amino acids 481–761, D2, dark blue) and C-domain (amino acids 762–806, grey) are indicated. Mutations detected in our three German IBMPFD patients affect evolutionarily highly conserved arginine residues in codon 93 and codon 155 of the CDC48 domain (red) (Modified from Hübbert et al., 2007).

A further pathogenic link of p97 to protein degradation pathways is highlighted by the observation that p97-positive protein aggregates have been documented in skeletal muscle and in neurons of the central nervous system of IBMPFD patients (Watts et al., 2004; Schröder et al., 2005). In neurons, these p97-positive inclusions are exclusively present in the nucleus, whereas in skeletal muscle only cytoplasmic p97-positive aggregates have been reported. However, p97-positive aggregates are not specific for IBMPFD and have been documented in a wide variety of neurodegenerative disorders comprising Parkinson's disease, Lewy Body disease, Huntington's disease, amyotrophic lateral sclerosis, and spinocerebellar ataxia type III (SCAIII; Machado-Joseph disease) (Hirabayashi et al., 2001; Mizuno et al., 2003; Nan et al., 2005). p97 directly interacts with ataxin-3, the protein mutated in SCAIII, and recent *in vivo* studies using *Drosophila* demonstrated that p97 selectively modulates aggregation and neurotoxicity induced by pathogenic ataxin-3 (Böddrich et al., 2006).

## **2.5. Clinical observations in patients involved in this study**

Clinical data and biopsy material from three German patients suffering from IBMPFD are included in this study (Schröder et al., 2005; Hübbers et al., Brain 2007). Clinical investigation of patients and probes derived from these patients was mainly done by R. Schröder before the start of this study.

Patient I is a 74-year-old male patient with a >20-year history of slowly progressive distal muscle weakness predominantly affecting the lower extremities and progressive cognitive impairment. Neurological examination showed marked generalized weakness and atrophy of distal arms and leg muscles. In addition, axial

weakness of the lumbar trunk was noticed. Repeated neuropsychiatric evaluation showed evidence of progressive personality changes and cognitive decline due to frontotemporal brain dysfunction. Axial computed tomography revealed Paget-like bone changes in the right hip. Mutation analysis revealed a novel heterozygous nucleotide substitution from arginin to cystein in exon 3 (p.Arg93Cys) of the p97 gene (GenBank AC004472; Hübbbers et al., 2007).

Patient II was a 62-year-old female patient harbouring of a progressive proximal muscle weakness and frontal and temporal brain atrophy leading to a severely demented patient with a flaccid, predominantly proximal tetraparesis. The mother of the reported patient, her mother's brother as well as one of his children suffered from similar medical conditions. She died of pneumonia and cardiac failure in 1998. Autopsy at that time showed severe generalized wasting of her skeletal muscles, but no signs of Paget's disease of the bone. The total heart weight was 480 g; left ventricular and right ventricular wall thickness was 1.7 and 0.7 cm, respectively. Neurons exhibited nuclear inclusions containing p97- and ubiquitin-containing material. A heterozygous mutation in exon 5 leading to an amino acid substitution from arginine to cystein in codon 155 was identified (p.Arg155Cys; Schröder et al., 2005). Additionally, mutations of the desmin and  $\alpha$ B-crystallin genes were ruled out by direct sequence analysis in this patient.

Patient III is a 54-year-old female. She gave a 30-year history of slowly progressive muscle weakness and atrophy predominantly affecting her shoulder girdle, trunk and distal leg muscles (Fig. 2A). Paget's disease of the bone confined to the first lumbar vertebra (Fig. 2B). A detailed neuropsychological evaluation suggested mild frontotemporal cognitive dysfunction. Neurological examination showed severe

weakness and atrophy of her scapular fixator muscles (deltoid, rhomboid, supra- and infraspinatus) and trunk extensors. In addition, she had slight to moderate muscle weakness of her finger extensor, hip flexor and distal leg muscles. Whole-body MRI demonstrated widespread muscular involvement with pronounced signal changes in her erector spinae, hamstring and calf muscles (Fig. 2C, D and E). p97 mutation analysis of a DNA sample revealed a heterozygous nucleotide substitution causing an amino acid substitution in the same codon as in patient II from arginine to histidine (p.Arg155His).



**Fig. 2. Clinical and MRI findings in Patient III.**

(A) The marked scapular winging and lumbar lordosis may be noted. (B) The sagittal view of the lumbar spine reveals a stripy ossification of the first lumbar vertebra (arrowhead) due to Paget's disease. T1-weighted TSE-sequence with 600/12 ms (TR/TE), 4 mm slice-thickness. (C) The cross-cut view at the level of the thoracic spine demonstrates a complete fatty replacement of the erector spinae muscles (\*). T1-weighted TSE-sequence with 450/17 ms (TR/TE), 5 mm slice-thickness. (D) The cross-cut view of the thighs shows a high degree of fatty degeneration of the right semimembranosus muscle (\*) and, to a lesser degree, of the left semimembranosus muscle (+). T1-weighted TSE-sequence with 450/17 ms (TR/TE), 5 mm slice-thickness. (E) MRI of the calves depicts marked fatty replacement of the left gastrocnemius muscle (\*) as well as signal changes in the anterior compartment muscles (+). T1-weighted TSE-sequence with 450/17 ms (TR/TE), 5 mm slice-thickness. (Hübbers et al., 2007)

## 2.6. Scientific questions and working plan

In summary this study was initiated to answer questions regarding the pathogenesis of the IBMPFD disease, which was described recently. To date, information about the complex pathology of the IBMPFD disease and experimental data about the cell biology and biochemistry were limited. To illuminate mechanisms that are involved in the development of this late onset and ultimately lethal disease, the following questions were addressed:

- What are the morphological and ultrastructural changes in the IBMPFD diseased striated muscle tissue?
- Does mutant p97 induce changes in its post-translational modification or subcellular localization?
- Can a cell culture model of the IBMPFD disease be established and do p97 overexpressing cells exhibit a phenotype similar to that of IBMPFD diseased tissue? Is a cell culture model capable to reproduce the formation of pathological protein aggregates?
- Are known pathways in which p97 is involved impaired by the p97 mutations? Are ERAD and proteasomal degradation activities affected?
- What are the consequences of p97 mutations on the molecule structure and which functional conclusions can be drawn out of it?

To address these questions, a variety of histological, molecular and cell biological, and *in silico* investigations were performed.

### **3. Results**

#### **3.1. Morphological, ultrastructural and biochemical analysis of the skeletal muscle and cardiac pathology**

##### *3.1.1. Skeletal muscle pathology*

Morphological evaluation of a vastus lateralis and tibial anterior biopsy from Patient I showed severe degenerative changes consisting of increased fibre size variation, atrophy of both fibre types, presence of terminal atrophic and angulated fibres, hypertrophic type-1 fibres, degenerating and a few regenerating fibres, 'myopathic grouping' as well as marked fatty replacement of muscle fibres and broadening of connective tissue (Fig. 3A). A diagnostic muscle biopsy taken from the biceps brachii muscle of Patient II displayed the classical myopathological picture of an IBM with an abundance of rimmed vacuoles (Fig. 3B). In contrast, the biopsy from the vastus lateralis muscle in Patient III showed only mild and unspecific myopathological changes consisting of type I fibre predominance, atrophic and hypertrophic fibres (Fig. 3C). In addition, few de- and regenerating fibres could be demonstrated. It is noteworthy that in biopsies from Patient I and III only a few fibres with rimmed vacuoles could be detected. None of the three reported cases showed inflammatory infiltrates.

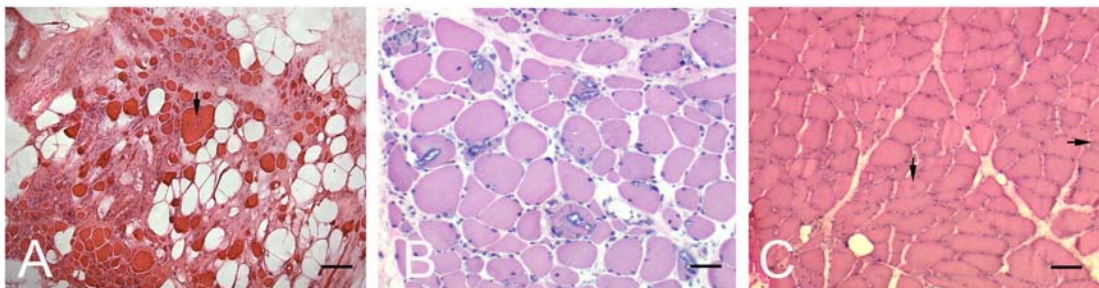


**Fig. 3. Morphological analysis of IBMPFD muscle.**

(A) Biopsy from Patient I revealed severe degenerative muscle changes. The marked fatty replacement of muscle fibres, broadening of connective tissue, rounding and atrophy of muscle fibres and hypertrophic fibres may be noted. The arrow denotes a hypertrophic fibre with a central rimmed vacuole. (B) Biopsy from Patient II showed the classical picture of an IBM with an abundance of rimmed vacuoles. (C) Biopsy from Patient III showed only mild and unspecific myopathological changes. Fibres containing rimmed vacuoles are marked by arrows. [Haematoxylin and Eosin staining; bars: (A) 100  $\mu\text{m}$ , (B) 50  $\mu\text{m}$ , (C) 60  $\mu\text{m}$ ].

Double-immunofluorescence analysis of skeletal muscle from Patient III revealed a small number of fibres (<5%) containing cytoplasmic foci of p97- and ubiquitin-positive protein aggregates (data not shown), whereas the corresponding analysis of the muscle biopsy from Patient II showed a high number of fibres (30-40%) with single or multiple p97- and ubiquitin-positive cytoplasmic inclusions (Fig. 4A and B). In addition, double-staining with p97 antibody and DAPI (4',6'-diamidino-2-phenylindole dihydrochloride) revealed multiple fibres with p97-positive nuclear inclusions (Fig. 4C and D). Further analysis revealed multiple fibres displaying subsarcolemmal and cytoplasmic areas with increased  $\alpha\text{B}$ -crystallin (Fig. 4E) and desmin labeling (Fig. 4F).

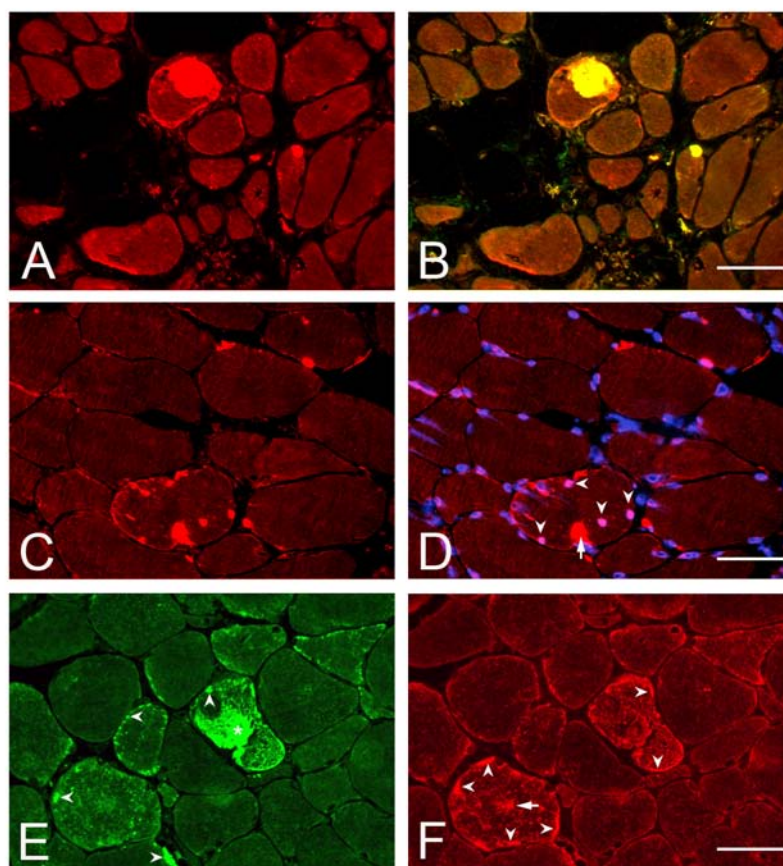


**Fig. 4. Indirect immunofluorescence analysis of IBMPF muscle from Patient II.** (A) p97 labeling of cytoplasmic aggregates. (B) p97 and ubiquitin double-immunofluorescence labeling of cytoplasmic aggregates. (C) p97 labeling of cytoplasmic and nuclear aggregates. (D) p97 and DAPI labeling. The presence of cytoplasmic (red, arrow) and nuclear (pink, arrowheads) aggregates may be noted. (E) Pathological  $\alpha$ B-crystallin staining with positive labeling of a giant cytoplasmic (\*) and multiple small subsarcolemmal aggregates (arrowheads). (F) Pathological desmin staining in two muscle fibres displaying increased subsarcolemmal (arrowheads) and cytoplasmic areas (arrow) with increased desmin immunolabeling. Bars: (B) 70  $\mu$ m, (D) 50  $\mu$ m, (F) 40  $\mu$ m.

A detailed ultrastructural analysis was performed on skeletal muscle from Patient II. The p97-positive nuclear inclusions consisted of filamentous material (Fig. 5A). In analogy to the abundance of rimmed vacuoles and cytoplasmic p97 and ubiquitin-positive inclusions at the light microscopic level, many fibres contained autophagic vacuoles with haphazardly arranged filamentous material as well as large cytoplasmic areas consisting of densely or loosely packed filamentous material

(Fig. 5B). Multiple fibres also displayed areas with granulo-filamentous material as seen in the group of myofibrillar myopathies (Fig. 5C). Immunogold EM showed a dense desmin-positive labeling of these areas (Fig. 5D).

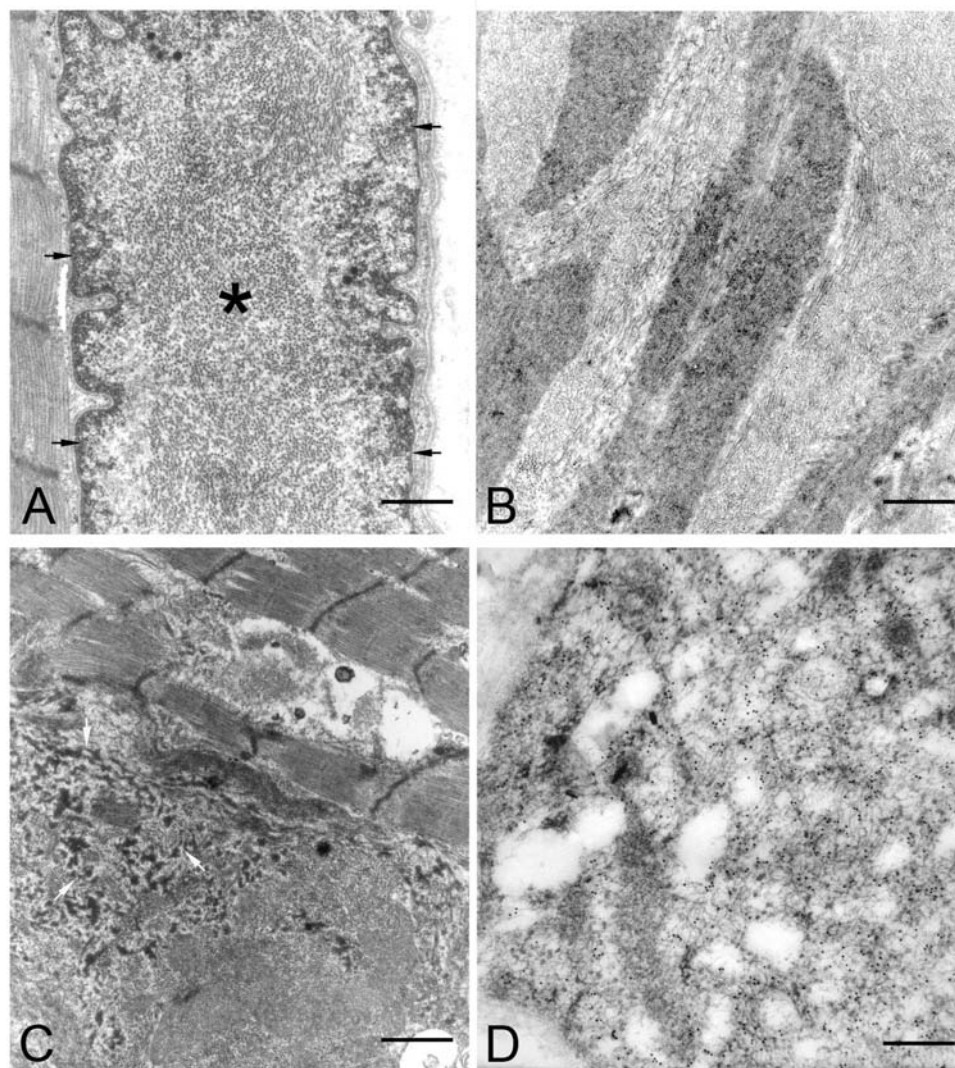


**Fig. 5. Ultrastructural analysis of skeletal muscle from Patient II.**

(A) Filamentous nuclear inclusion (\*); arrows indicate the nuclear membrane. (B) Cytoplasmic area with loosely and densely packed filamentous material. (C) The arrows denote an area with granulo-filamentous material. (D) Immunogold electron microscopy with the monoclonal anti-desmin antibody (mab-D33) and a secondary antibody coupled to 10 nm gold particles showed a dense labeling of filamentous aggregates. Bars: (A) 0.5  $\mu\text{m}$ , (B) 0.6  $\mu\text{m}$ , (C) 0.7  $\mu\text{m}$ , (D): 0.25  $\mu\text{m}$ .

### 3.1.2. Cardiac pathology

Post-mortem analysis of the heart of Patient II revealed a marked left ventricular dilatation and thickening of the left ventricular wall (Fig. 6A). Histopathological examination showed cellular hypertrophy of myocytes and in conjunction with multiple small parenchymal scars in both ventricles. Immunostaining of formalin-fixed and paraffin-embedded cardiac tissue revealed multiple cardiomyocytes displaying ubiquitin-positive cytoplasmic and single nuclear inclusions (Fig. 6B and C).



**Fig. 6. Cardiac pathology in IBMPFD.**

(A) Post-mortem image of the heart from Patient II displaying left ventricular dilatation (\*) and thickening of the left ventricular wall (brace). (B and C) Ubiquitin immunostaining of cardiac muscle tissue. The presence of cytoplasmic (arrows) and intranuclear (arrowhead) ubiquitin-positive inclusions may be noted. (B and C) Alkaline phosphatase anti-alkaline phosphatase staining (APAP). Bars: (B) 50  $\mu\text{m}$ , (C) 15  $\mu\text{m}$ .

### 3.1.3. p97 protein expression in IBMPFD muscle

We performed 1D- and 2D-SDS-PAGE in conjunction with western blotting of total protein extracts of normal and diseased (R93C, R155H, R155C) skeletal muscle. p97 immunoblotting after 1D-SDS-PAGE revealed a single band corresponding in size to 97 kDa in all samples analysed without significant changes in the total amount of p97 between normal and R93C-, R155H-, R155C-IBMPFD muscle (Fig. 7). A previous study reported a shift of p97 from the soluble to the pellet fraction in

transient transfection experiments using p97-R155H-GFP and p97-R95G-GFP constructs (Weihl et al., 2006). To study the distribution of p97 between soluble and insoluble muscle protein fractions, we performed differential centrifugation of muscle tissue lysates. However, in IBMPFD and normal control muscle p97 was exclusively found in the pellet fraction of IBMPFD and normal control muscle (Fig. 7).

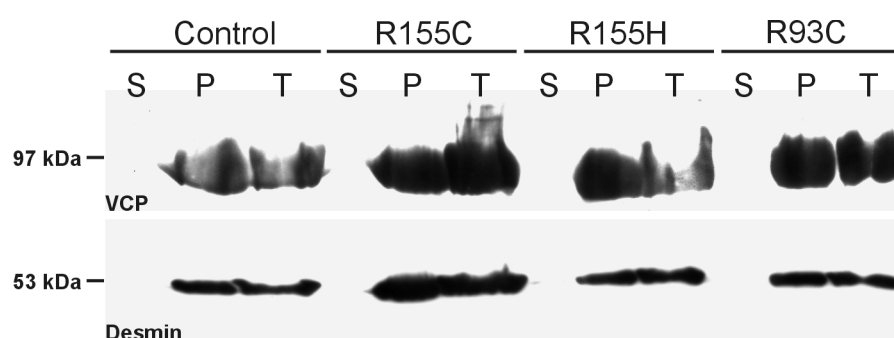


**Fig. 7. p97 immunoblot analysis of normal and IBMPFD muscle after differential centrifugation.**

Western blotting of equal amounts of total protein extracts (T), soluble (S), and pellet fractions (P) from normal (Control) and diseased (R155C, R155H, R93C) skeletal muscle after centrifugation at 100.000 x g. Desmin labeling (53 kDa) was used as an internal loading control. p97-immunoblotting detected a single band corresponding to a molecular weight of ~97 kDa in pellet and total protein fractions of all probes analysed.

p97 immunoblotting after 2D gel electrophoresis of total protein extracts from normal human skeletal muscle revealed a prominent spot at pH 5.20. In addition, a second spot with reduced signal intensity was detected at the position of pH 5.16, which corresponds well with the calculated pI 5.14. A corresponding analysis of diseased skeletal muscle (R155C) showed an identical pattern compared to the normal human control muscle (Fig. 8).

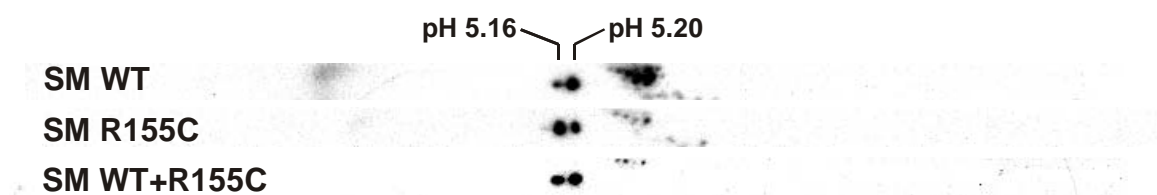


**Fig. 8. 2D gel electrophoresis followed by p97 indirect immunoblot analysis of total protein extracts from normal and diseased (R155) human skeletal muscle.**  
A mixture of both samples was loaded as internal control to confirm that the detected spots of normal and diseased proteins correspond to each other.

#### 3.1.4. Analysis of normal and IBMPFD primary human myoblasts

In order to study pathological protein aggregate formation in cultured cells, we analysed normal and IBMPFD (R155C-p97 mutant) primary human myoblasts. Immunostaining using FK2 (Fig. 9C, D) and p97 antibodies (data not shown) revealed an identical reticular staining pattern in normal and IBMPFD myoblasts. In contrast to IBMPFD muscle, no pathological protein aggregate formation could be detected. Even treatment with *clasto*-lactacystin  $\beta$ -lactone (irreversible 20S proteasome inhibitor) or MG132 (reversible 26S proteasome inhibitor) did not induce protein aggregates (Fig. 9E – H).

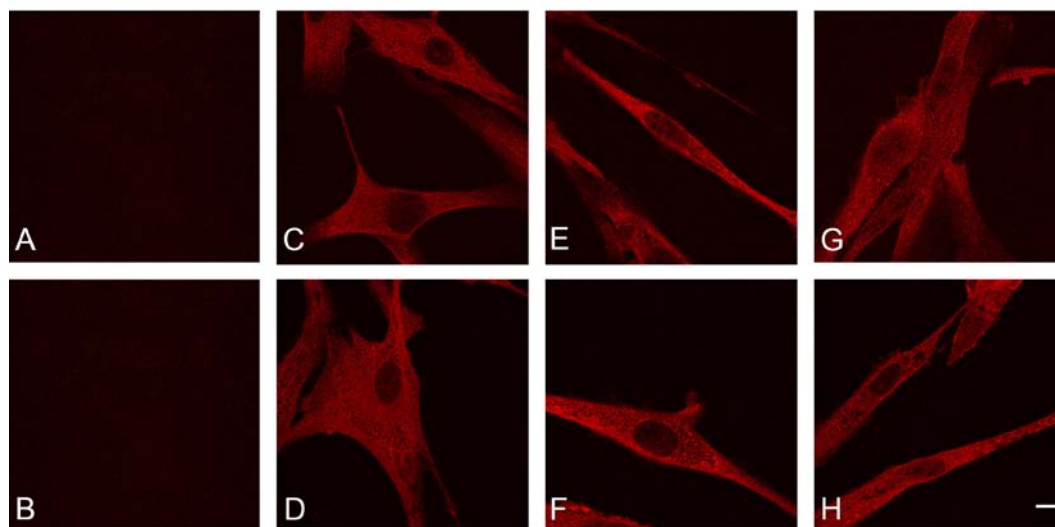


**Fig. 9. Confocal immunofluorescence images of IBMPFD (A, C; E and G; R155C) and normal (B, D, F and H) primary human myoblasts.**

Cells were stained with an antibody directed against poly-ubiquitin (FK2). (A and B) Controls lacking the primary antibody. (C and D) untreated cells, (E and F) MG132 treated cells, (G and H) Lactacystin treated cells. Note that both normal and IBMPFD myoblasts display an identical reticular FK2-staining pattern without any evidence of FK2-positive protein aggregates in treated and untreated cells; bar, 20  $\mu$ m.

We also performed indirect immunoblotting after gel electrophoresis of untreated total cell lysates from these primary myoblasts (Fig. 10). p97 staining (upper panel) showed equal signals for both mutated and control muscle, thus indicating that there is no obvious influence of the mutation on the total amount of p97 protein expression. Desmin (middle panel) was used to confirm the myoblast nature of the primary cells and as an internal loading control, respectively.  $\beta$ -actin (lower panel) was used as an additional internal loading control.

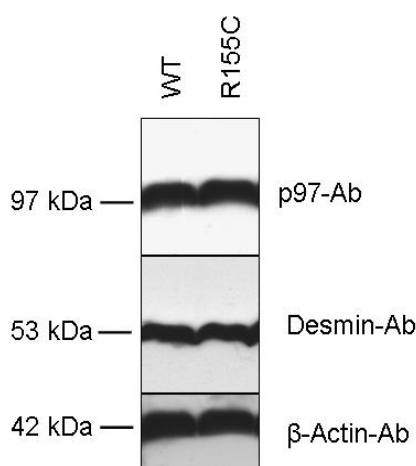


**Fig. 10. Immunoblot analysis of total protein extracts from cultured normal and IBMFPD (R155C-p97 mutant) primary myoblasts.**

*Note the equal p97 signal intensities in samples from normal and IBMFPD myoblasts. Desmin was used to confirm the myoblasts nature of the primary cells and as an internal loading control, respectively. In addition,  $\beta$ -Actin was used as an internal loading control.*

### **3.2. Generation and characterization of wt and mutant p97 constructs**

We generated wild type and mutant (R93C, R155C, R155H) cDNA constructs to study the effects of p97 protein mutants at the cellular level (Fig. 11). The following transfection and transduction experiments were performed: (i) Wt- and mutant-GFP-p97-FLAG and p97-FLAG-GFP were transiently and stably expressed in HEK293 cells; (ii) wt- and mutant-p97-FLAG-GFP were transiently expressed in C2F3 myoblasts; (iii) wt- and the R155C-p97-FLAG mutant were stably expressed in C2F3 myoblasts.

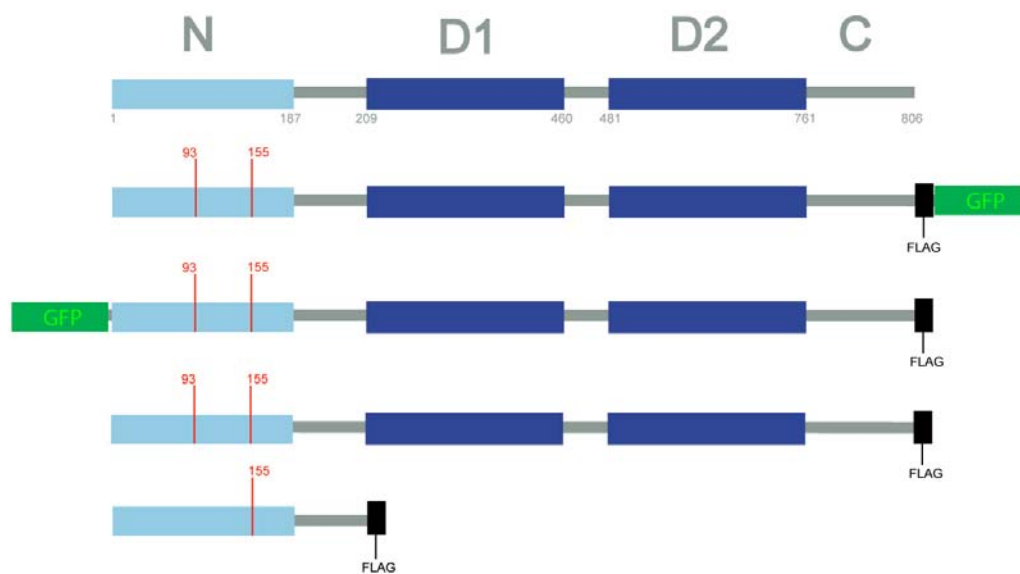


**Fig. 11. Schematic representation of constructed p97 vectors.**

Upper panel: Representation of the endogenous p97 protein. Panel 2 – 4: Full length p97 constructs for the expression of wt, R93C, R155C, and R155H proteins were constructed with an additional FLAG-Tag at the C-terminus (all constructs) and a GFP was fused to the C-terminus (2) or N-terminus (3) for fluorescence detection. Lower panel: Partial p97 construct for the expression of the first 208 amino acids of wt, R155C and R155H protein representing the N-domain and the N-D1 linker were fused to a FLAG-tag.

### 3.2.1. Immunofluorescence analysis of p97 overexpressing cells

Transfected cells were analysed by live cell imaging and indirect immunofluorescence analysis after methanol or paraformaldehyde fixation. Expression of either wt-p97-constructs in HEK293 cells resulted in an intense labeling of the entire cytoplasm and, inconsistently, in a less intense nuclear signal of the GFP fusion proteins (Fig. 12A-O and Fig. 13A-O). All N- or C-terminally tagged full-length mutant p97 constructs showed the same localization as endogenous p97, with no evidence of abnormal cytoplasmic protein aggregate formation in HEK293 and C2F3 cells, as it was presented earlier by Weihl et al. (2006). Transfection of

GFP alone yielded in a strong uniform labeling of both the cytoplasm and the nucleus (Fig. 12A, F, K and Fig. 13A, F, K).

To address the issue of protein aggregate formation in a more physiological setting, we performed stable transfections of HEK293 and C2F3 cells. Two months after the initial transfection, cells were analysed by life cell imaging. The localization of the three p97 mutants again was indistinguishable from wt-p97, with no evidence of protein aggregate formation (data not shown). Triton X-100 treatment before or after fixation of HEK293 cells did not unmask any protein aggregates (data not shown). Additionally, we performed indirect immunofluorescence analysis of the transfected HEK293 cells using antibodies directed against p97, FLAG and poly-ubiquitinated proteins (FK2). Here, p97 (Fig. 12P-T and Fig. 13P-T) and FLAG (data not shown) labeling showed a pattern analogous to N- or C-terminally GFP- or FLAG-tagged wt- and mutant-p97 constructs in living and fixed cells. The FK2 antibody, a sensitive marker for pathological aggregates containing poly-ubiquitinated proteins, showed a diffuse cytoplasmic staining with occasional small foci displaying accentuated FK2 immunolabeling in the cytoplasm and nucleus of non-transfected (data not shown) as well as transfected (wt-, R93C-, R155H-, R155C-p97) HEK293 cells (data not shown).

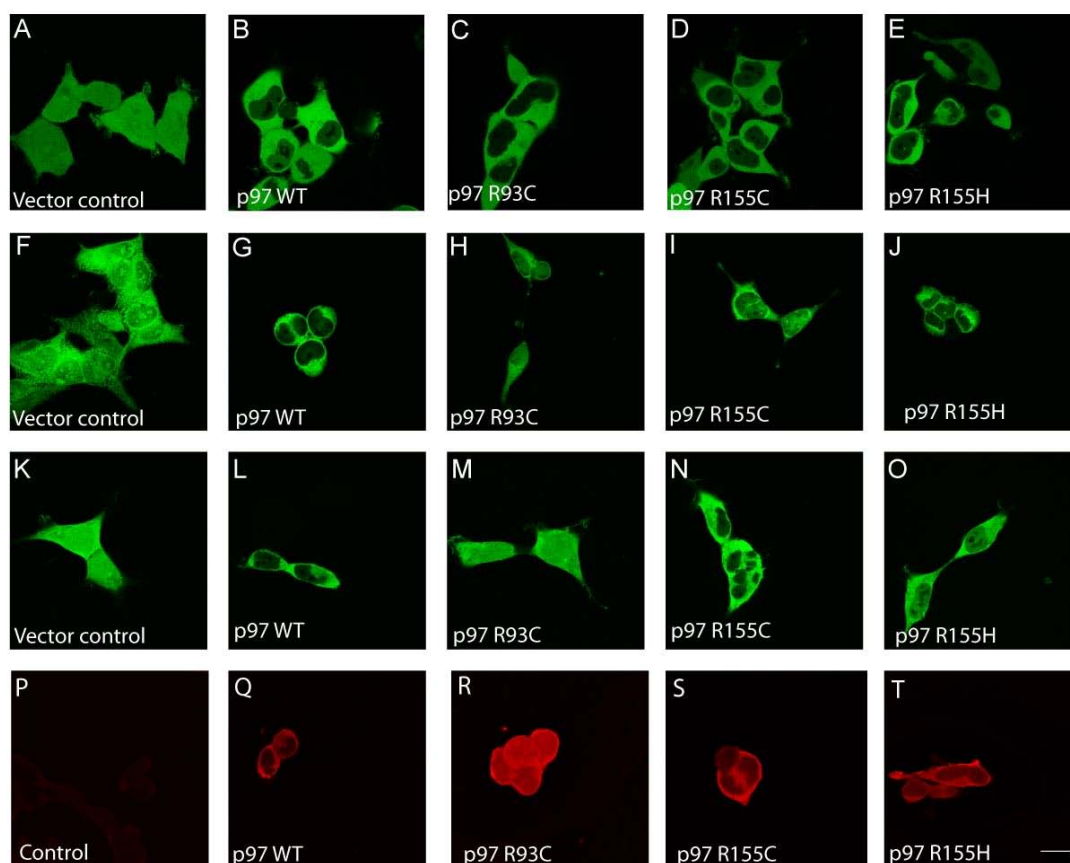


**Fig. 12. Confocal images of HEK293 cells stably overexpressing wt- or mutant p97 protein fused to N-terminal GFP.**

(A – E) Living cells, GFP signal; (F – J) Methanol fixation, GFP signal; (K – O) Paraformaldehyde fixation, GFP signal; (P-T) Indirect immunofluorescence of paraformaldehyde fixed cells, p97 staining. (A) GFP Vector control, (B) GFP-wt-p97-FLAG, (C) GFP-R93C-p97-FLAG, (D) GFP-R155C-p97-FLAG, (E) GFP-R155H-p97-FLAG. (F) GFP Vector control, (G) GFP-wt-p97-FLAG, (H) GFP-R93C-p97-FLAG, (I) GFP-R155C-p97-FLAG, (J) GFP-R155H-p97-FLAG. (K) GFP Vector control, (L) GFP-wt-p97-FLAG, (M) GFP-R93C-p97-FLAG, (N) GFP-R155C-p97-FLAG, (O) GFP-R155H-p97-FLAG, (P) p97 staining control lacking primary antibody, (Q) GFP-wt-p97-FLAG, (R) GFP-R93C-p97-FLAG, (S) GFP-R155C-p97-FLAG, (T) GFP-R155H-p97-FLAG. Bar, 20  $\mu$ m.

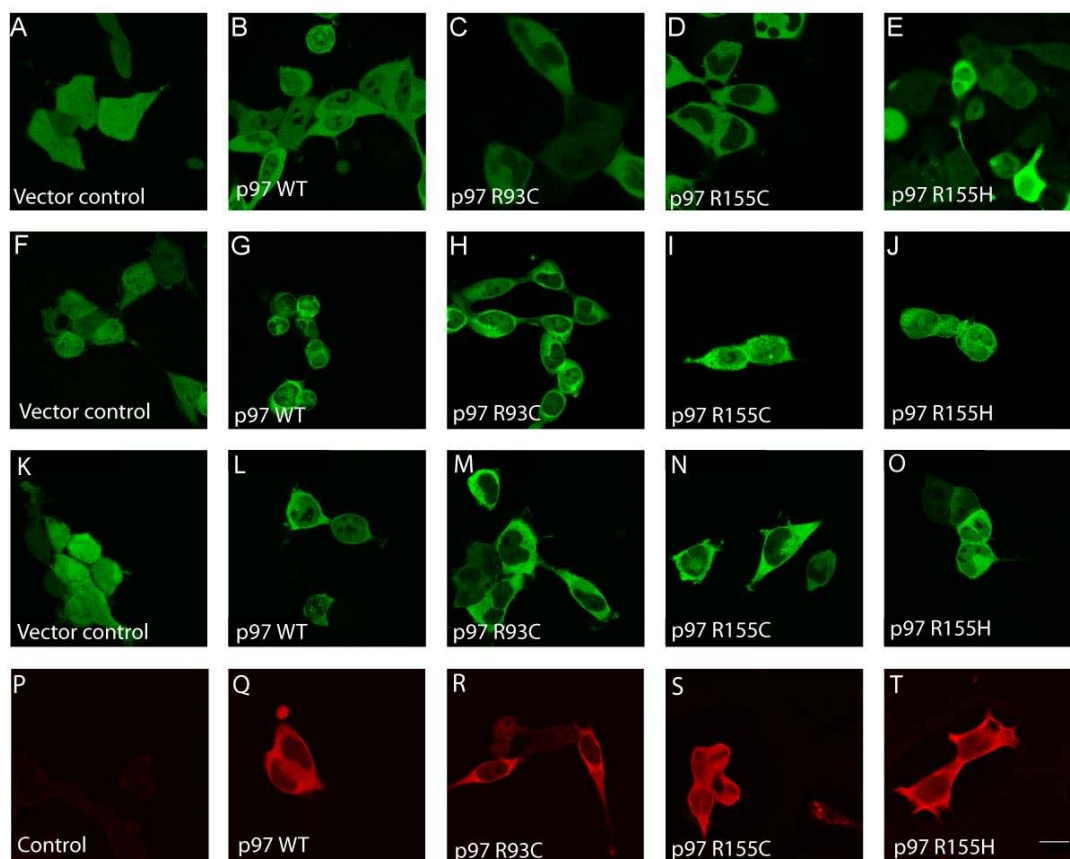


**Fig. 13. Confocal images of HEK293 cells stably overexpressing wt- or mutant-p97 protein fused to a C-terminal GFP.**

(A – E) Living cells, GFP signal; (F – J) Methanol fixation, GFP signal; (K – O) Paraformaldehyde fixation, GFP signal; (P-T) Indirect immunofluorescence of paraformaldehyde fixed cells, p97 staining. (A) GFP Vector control, (B) wt-p97-FLAG-GFP, (C) R93C-p97-FLAG-GFP, (D) R155C-p97-FLAG-GFP, (E) R155H-p97-FLAG-GFP, (F) GFP Vector control, (G) wt-p97-FLAG-GFP, (H) R93C-p97-FLAG-GFP, (I) R155C-p97-FLAG-GFP, (J) R155H-p97-FLAG-GFP, (K) GFP Vector control, (L) wt-p97-FLAG-GFP, (M) R93C-p97-FLAG-GFP, (N) R155C-p97-FLAG-GFP, (O) R155H-p97-FLAG-GFP, (P) p97 staining control lacking primary antibody, (Q) wt-p97-FLAG-GFP, (R) R93C-p97-FLAG-GFP, (S) R155H-p97-FLAG-GFP, (T) R155C-p97-FLAG-GFP. Bar, 20  $\mu$ m.

In order to rule out effects of the GFP-tag, we retrovirally transduced C2F3 (a subclone of C2C12) myoblasts using wt-p97-FLAG and R155C-p97-FLAG expression constructs. Anti-FLAG- (Fig. 14C and D) and anti-p97-staining (data not shown) revealed an intense labeling of the entire cytoplasm and, inconsistently, a less intense nuclear signal. Transduced C2F3 cells differentiated into myotubes showed the same results (Fig. 14E and F). However, neither myoblasts nor up to 6-day-old myotubes showed any evidence of protein aggregates.

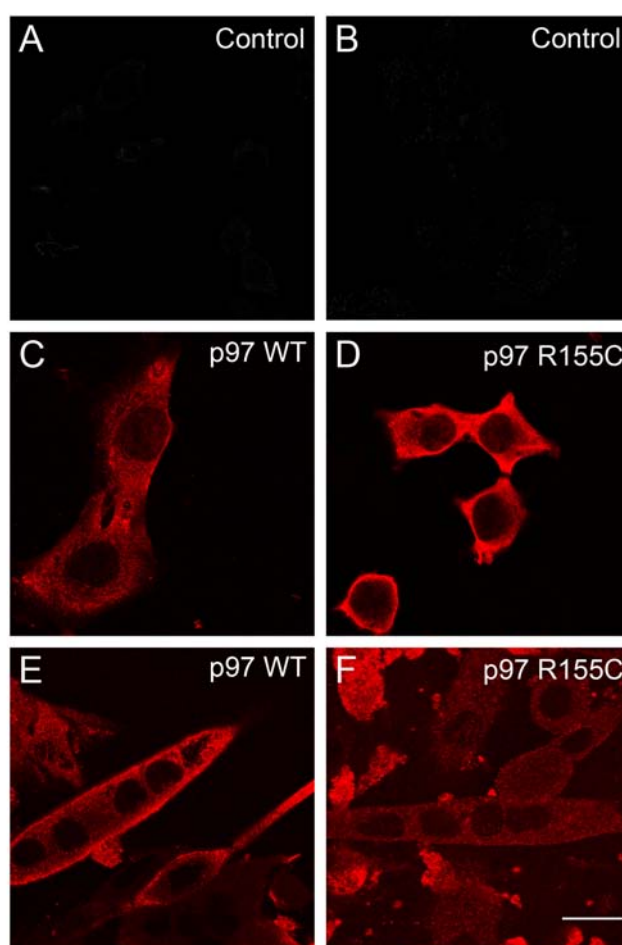


**Fig. 14. Confocal immunofluorescence images of retrovirally transduced C2F3 myoblasts and myotubes overexpressing wt- or mutant-p97-FLAG protein.**

Cells were stained with an antibody directed against the FLAG-epitope. Controls, immunofluorescence images of untransduced cells (A) and of wt-p97-FLAG expressing myoblasts lacking the primary antibody (B). Distribution of wt-p97-FLAG in myoblasts (C) and differentiated myotubes (E). Localization of R155C-p97-FLAG in myoblasts (D) and differentiated myotubes (F); bar, 20  $\mu$ m.

The N-domain of p97 is reported to be crucial for cofactor-binding. To induce possible dominant negative-like effects, we also generated p97 plasmids for stable expression of the first 208 amino acids of the N-terminus of p97 (Fig. 11; wt, R155H and R155C) and analyzed HEK293 cells for possible differences in the localization of the wild type and mutant N-terminal peptides (Fig. 15). Indirect immunofluorescence analysis of paraformaldehyde fixated cells showed an intense labeling of the cytoplasm with no apparent differences between wt and mutant p97 and, especially, no hints for aggregate formation.

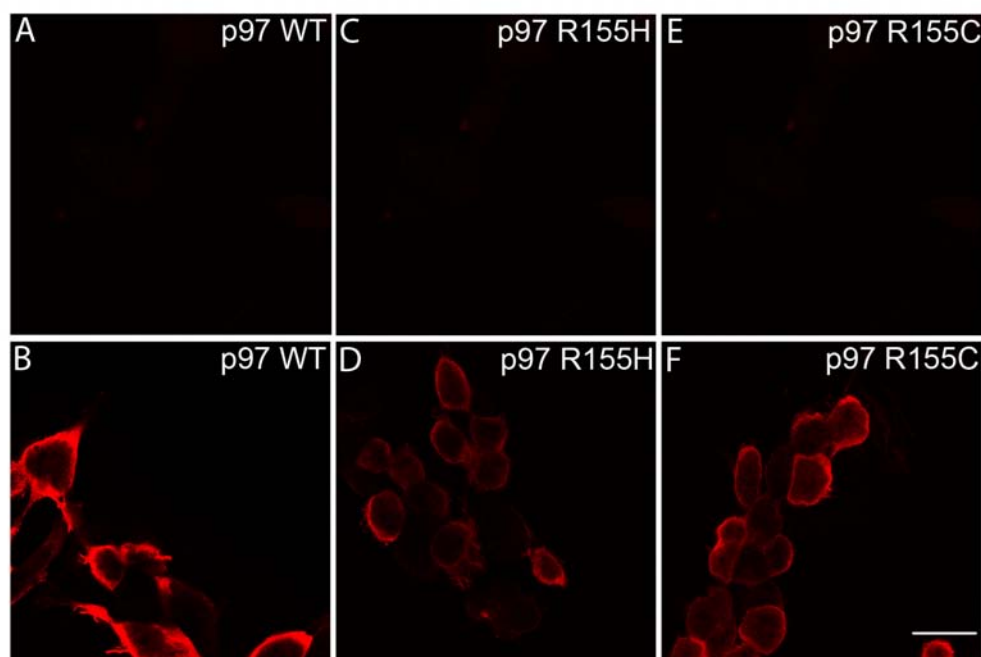


**Fig. 15. Confocal immunofluorescence images of transfected HEK293 cells overexpressing wt and mutant N-terminal peptide fragments of p97.**

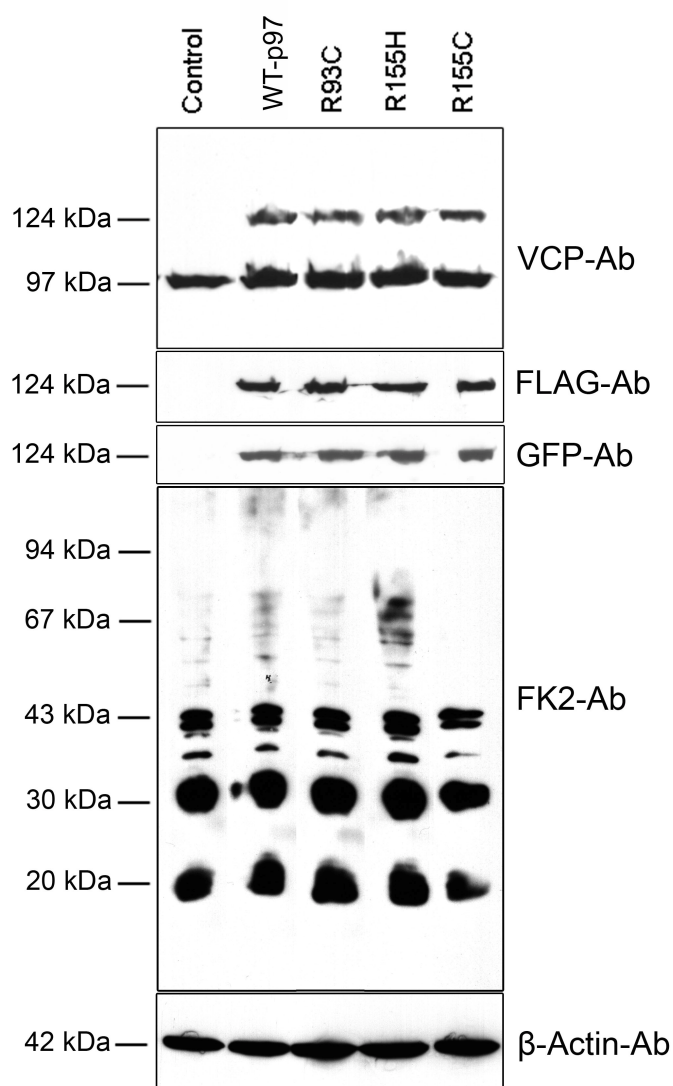
Cells were stained with an antibody directed against the FLAG-epitope. Controls, immunofluorescence images of cells stained with secondary antibody only (A, C, E). Distribution of N208-wt-p97-FLAG (B), N208-R155H-p97-FLAG (D) and N208-R155C-p97-FLAG (F); bar, 20  $\mu$ m

3.2.2. *1D- and 2D SDS-PAGE followed by immunoblotting of p97 overexpressing cells and primary myoblasts*

For further biochemical analysis of our transfected HEK293 cells, we performed immunoblotting of total protein extracts using p97, GFP, FLAG and FK2 antibodies (Fig. 16). p97 immunoblotting labelled the endogenous p97 protein as well as the GFP-p97 fusion protein. The GFP and FLAG antibodies exclusively detected the respective fusion proteins. Comparison of signal intensities indicated an endogenous p97 to wt-, R93C-, R155H and R155C-p97 fusion protein ratio of 3:1.

***Fig. 16. (Page 34) Western blot analysis of HEK293 total protein extracts from non-transfected and transfected cells as indicated.***

*$\beta$ -Actin was used as an internal loading control (lower panel). The ratio of 3:1 of endogenous versus GFP-fusion proteins (upper panel) may be noted. Poly-ubiquitin western blotting (FK2) revealed no significant differences in the pattern of immunolabelled proteins in all samples analyzed. Western blotting against FLAG-epitope and GFP-tag exclusively labelled transfected p97 proteins at predicted sizes.*



Immunoblotting after differential centrifugation of cell lysates showed that both the endogenous p97 and wt-, R93C-, R155H-, R155C-p97 fusion proteins are almost exclusively present in the soluble fraction (data not shown). To analyse whether ubiquitinated proteins accumulate in the cells expressing mutant-p97, we performed immunoblotting using the FK2 antibody. Here, identical patterns of poly-ubiquitinated proteins were observed in all samples analysed (data not shown).

p97 immunoblotting after 2D gel electrophoresis of total protein extracts from wt-p97-FLAG and R155C-p97-FLAG transduced C2F3 myoblasts differentiated into

myotubes showed an identical pattern to the one in normal and IBMPFD muscle (Fig. 17).

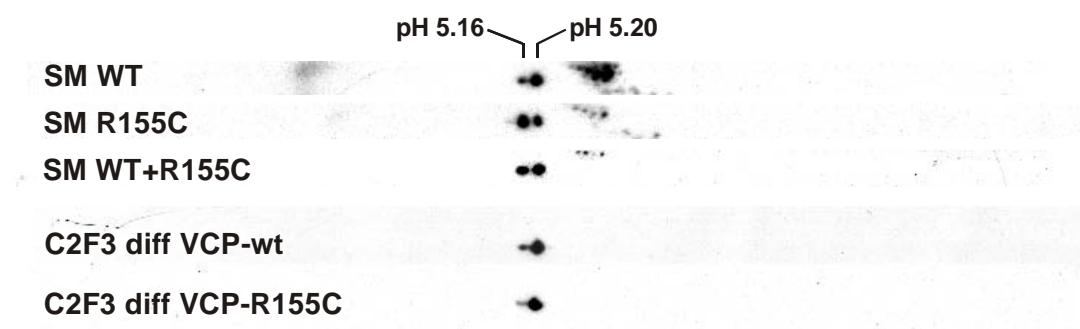


**Fig. 17. 2D gel electrophoresis and indirect p97 immunoblotting of total protein extracts of normal and IBMPFD skeletal muscle and differentiated C2F3 cells overexpressing wt and R155C p97.**

The IBMPFD skeletal muscle analysis from Fig. 8 is shown for better comparability. A mixture of both skeletal muscle samples was loaded as internal control to confirm that the detected spots of normal and diseased proteins correspond to each other.

Expression of N208-p97-wt-FLAG, N208-p97-R155H-FLAG, and N208-p97-R155C-FLAG (predicted molecular mass: 25 kDa) was confirmed by western blot analysis using p97 and FLAG specific antibodies (Fig. 18). No changes to the full length situation were obvious.

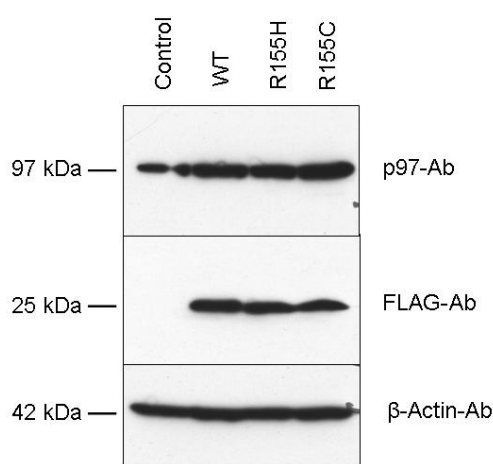


**Fig. 18. Western blot analysis of total protein extracts from non-transfected and transfected HEK293 cells overexpressing the N-terminal 208 amino acids.**

$\beta$ -Actin was used as an internal loading control (lower panel), N-terminal peptides were detected by the FLAG-epitope (middle panel), endogenous p97 was detected by p97 antibody (upper panel).

### 3.2.3. Cell proliferation assay

Cell proliferation assay showed that cells which were stably overexpressing wt-p97 and R155C-p97 decreased the cell growth as compared to untransduced C2F3 myoblasts or untransfected HEK293 cells. However, no significant difference had been found between the cells stably overexpressing wt-p97 and R155C-p97 (Fig. 19).

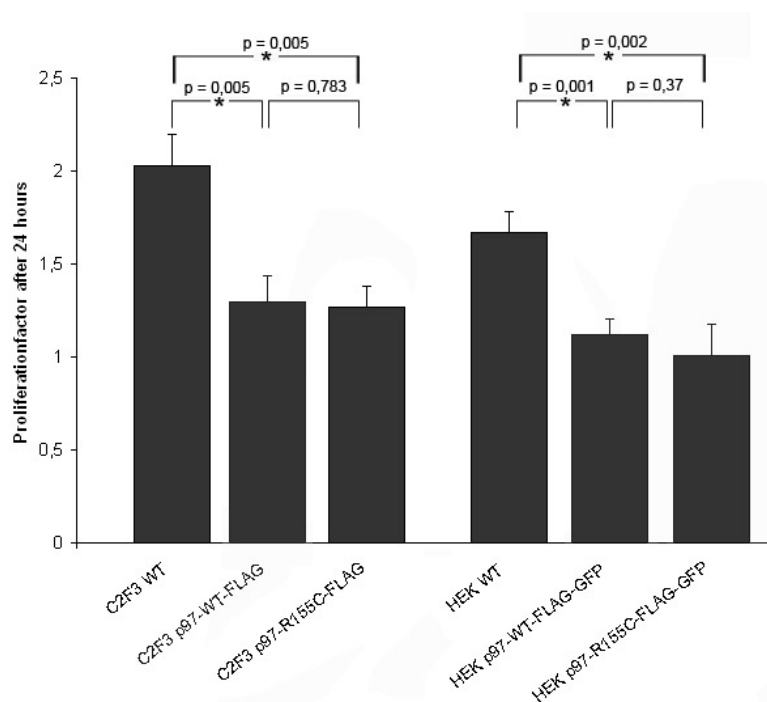


**Fig. 19. Cell proliferation assay of untransduced and transduced C2F3 cells and untransfected and transfected HEK293 cells as indicated.**

Overexpression of p97 leads to an approximately 1/3 decrease of proliferation in comparison to untransduced and untransfected cells.  $1 \times 10^6$  cells were seeded initially, cells were counted again after 24 hours. Significance values were assigned using unpaired students T-Test.

### 3.3. p97 response to cellular stress

#### 3.3.1. Use of various cell stressors to induce p97 aggregates

IBMPFD patients show a severe phenotype with pathological intracellular protein aggregates in diseased tissues. These cellular damages occur in postmitotic cells and need several decades to accumulate. In transient and stable transfection studies using mutated p97 constructs no protein aggregation pathology could be observed. In order to analyze the influence of various cell stressors, stably transfected and non-transfected HEK293 cells were treated with mitomycin C (DNA-alkylating agent), UV radiation (DNA and protein cross-linking), H<sub>2</sub>O<sub>2</sub> (oxidative stress), osmotic shock, wortmannin (PI3-kinase inhibitor), *clasto*-lactacystin  $\beta$ -lactone (irreversible 20S proteasome inhibitor) or MG132 (reversible 26S proteasome inhibitor). Changes in the subcellular p97 distribution of stably transfected cells were only observed in response to MG132 treatment. In C-terminally GFP-tagged wt-p97- or R93C-, R155H-, R155C-p97 cells treatment with this reversible 26S proteasome inhibitor resulted in the formation of a single perinuclear aggregate with marked GFP signal intensity in most of the cells analyzed (Fig. 20G, I, K, M). However, these protein aggregates showed no presence of poly-ubiquitinated proteins (labeling with the FK2 antibody) (Fig. 20H, J, L, N) and they also did not exhibit F-actin cytoskeleton (phalloidin staining) (data not shown). Furthermore, 80% of the cells additionally displayed few small foci of intranuclear protein aggregates.

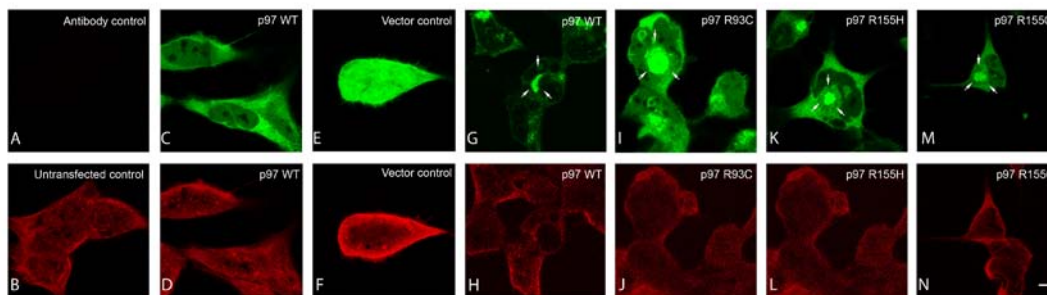


**Fig. 20. Confocal immunofluorescence images of HEK293 cells stably overexpressing wt- or mutant-p97-FLAG-GFP.**

(A-D) non-treated or (E-N) treated by MG132 (green = GFP; red = poly-ubiquitin, FK2-antibody). (A), wt-p97-FLAG-GFP transfected HEK293 cells stained with secondary antibody only. (B), untransfected HEK293 cells stained with the FK2 antibody. (C,D), untreated cells overexpressing wt-p97-GFP, and treated HEK293 cells expressing GFP only (E,F) did not display any protein aggregation. The use of MG132 resulted in the formation of marked perinuclear p97-positive aggregates (arrows) in wt-p97-GFP (G,H), R93C-p97-GFP (I, J), R155H-p97-GFP (K, L) and R155C-p97-GFP (M, N) cells. Note, that the p97-positive aggregates lack FK2-staining; bar, 40  $\mu$ m.

### 3.3.2. Time course of aggregate formation and clearance

In order to analyze the fate of aggregates, we examined aggregate formation and clearance in HEK293 cells stably overexpressing R155C-p97-FLAG-GFP and wt-p97-FLAG-GFP. When these cells were treated with the reversible proteasome inhibitor MG132, approximately 3/4 of the cells exhibited a perinuclear aggregate. The proteasomal inhibitor MG132 was washed away from the cells by changing the cell culture medium. Investigation of proteasomal activity recovered cells throughout the next days showed that both wt- and R155C-p97 overexpressing cells could clear the protein aggregates. However, there was a significant delay of protein aggregate clearance in HEK293 cells stably overexpressing R155C-p97-FLAG-GFP as compared to wt-p97-FLAG-GFP. To pinpoint the cause for delaying protein

aggregate clearance in mutant p97, stably transfected cells overexpressing wt-p97 and R155C-p97 were seeded on coverslips for 12 h. Subsequently cells were incubated with CDK4 inhibitor (2-Bromo-12,13-dihydro-5H-indolo[2,3-a]pyrolo[3,4-c]carbazole-5,7(6H)-dione; Calbiochem; inhibits the cell cycle at the G1 phase of cell division) to maintain constant number of cells for the quantitative analysis of aggregate degradation activity. Cells were subjected to the proteasome inhibitor MG132 for 16 h followed by recovering its activity. To monitor the proteasomal activity in different time periods, cells were collected every 12 h and fixated with paraformaldehyde and subsequently analysed by fluorescence microscopy. Protein aggregate clearance was dramatically decreased after 36 h of proteasomal inhibitor removal in cells stably overexpressing R155C-p97 (Fig. 21). Wt-p97 overexpressing cells showed approximately 4,5% remaining aggregates and mutant p97 overexpressing cells still contained a significantly higher level of 23,1% aggregates ( $p=0,045$ ). 48 hrs after recovering proteasomal activity, both wt- and mutant p97 overexpressing cells showed a similar low level of remaining aggregates (3,2% vs. 3,3%), which did not further decrease in the next up to 24 hours (data not shown). The number of cells seeded for this experiment remained nearly constant throughout the experiment (data not shown). Both DMSO and CDK4 inhibitor were ruled out to induce aggregates or to negatively influence treated cells by investigating them throughout 84 h (data not shown).

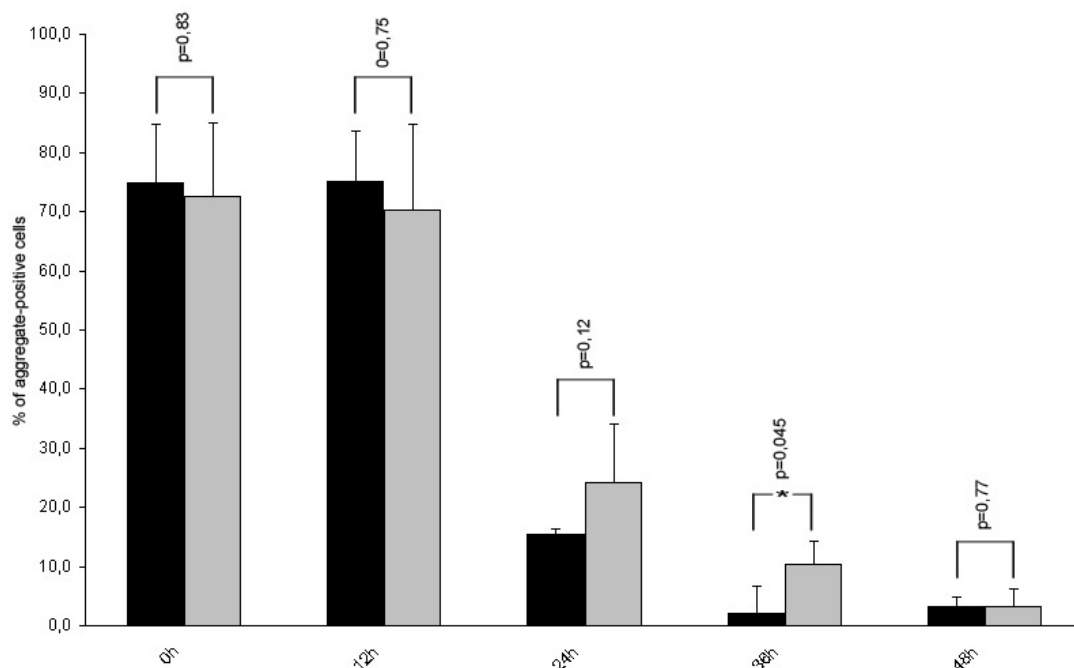


**Fig. 21. Time course experiment of aggregate clearance after proteasome inhibition.**

*HEK293 cells overexpressing wt-p97-FLAG-GFP (black) and R155C-p97-FLAG-GFP (grey) were arrested in G1 phase of the cell cycle by addition of a CDK4 inhibitor throughout the whole experiment. Proteasomal activity was inhibited by incubation with MG132 for 16 h. Time points indicated give the time span after removal of the reversible proteasome inhibitor MG132. Bars show percentage of cells containing aggregates in relation to total amount of cells counted. Each experiment was performed four times independently and 10 randomly chosen viewing fields were counted in each experiment. The significant delay in aggregate clearance for mutant p97 36 h after reactivating the proteasome may be noted. Significance values were assigned using unpaired students T-Test.*

### 3.4. Study of proteasome and ERAD activities

#### 3.4.1. Proteasomal activity

p97 along with its cofactors is closely related to proteasomal activity. To examine the putative involvement of mutant p97 in a proteasomal dysfunction, we measured the peptidase activity of proteasomes from untransfected and wt-p97-FLAG-GFP and R155C-p97- FLAG-GFP overexpressing HEK293 cells. Cell lysates were prepared from untransfected and transfected cells and centrifugated at 1.000 x g. The

supernatant was incubated with fluorogenic peptide substrates, which are specific for the three major peptidase activities (N-Suc-LLVY-7-amino-4-methylcoumarin-AMC for chymotrypsin-like activity, Z-AAR-AMC for trypsin-like activity, and Z-LLE-7-AMC for caspase-like activity) (Fig. 22A). Measurements were performed in presence or absence of respective proteasome inhibitors (Epoxomicin, inhibits chymotrypsin-like activity; Adamantaneacetyl-(6-aminohexanoyl)3-(leucinyloxy)3-vinyl-(methyl)-sulfone, inhibits all three major peptidase activities) which were used to ruled out other peptidase activities (data not shown). We found that the proteasomal activity had been increased in HEK293 cells stably overexpressing wt-p97-FLAG-GFP as compared to R155C-p97-FLAG-GFP and untransfected cells. However, there was a significant amount of proteasomal activity decreased in the case of cells stably overexpressing mutant R155C-p97-FLAG-GFP and its activity was lower than in untransfected cells. Also immunoblotting with anti- $\beta$ -actin and anti-p97 confirmed that the amount of total protein and wt- and R155C-p97 was equal (Fig. 22B). The R155C mutation of p97 seems to inhibit the overall proteasomal activity. This finding will be further investigated using transfected myoblasts and primary myoblasts as well as samples of skeletal muscle biopsies derived from the IBMPFD patients.

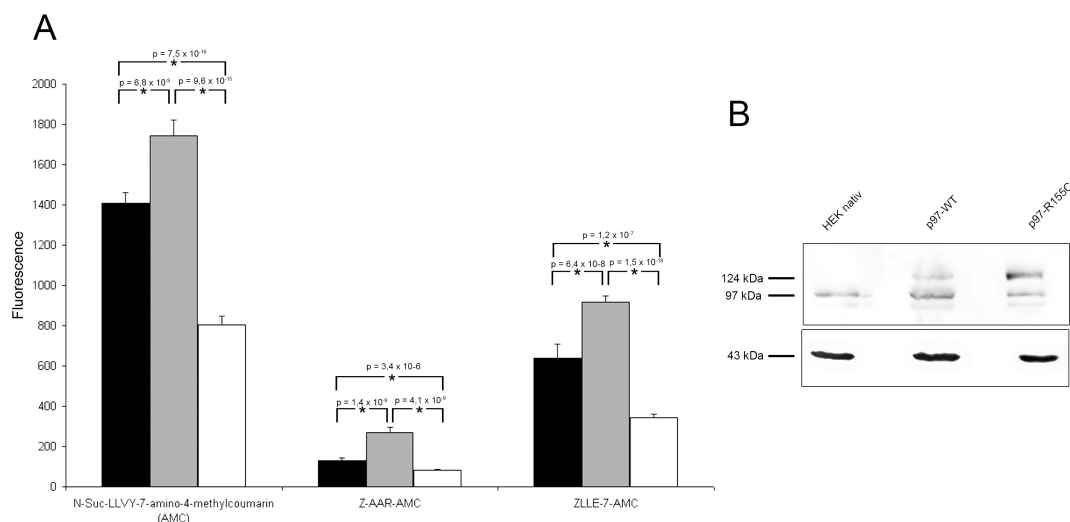


**Fig. 22. Analysis of proteasomal activity of untransfected and transfected HEK293 cells overexpressing wt- and R155C-p97-FLAG-GFP.**

(A) Cell lysates of untransfected HEK293 cells (black), stably transfected HEK293 cells overexpressing wt-p97-FLAG-GFP (grey) and R155C-p97-FLAG-GFP (white) were incubated with synthetic, fluorogenic proteasome substrates (N-Suc-LLVY-7-amino-4-methylcoumarin-AMC for chymotrypsin-like activity, Z-AAR-AMC for trypsin-like activity and Z-LLE-7-AMC for caspase-like activity). Cells were counted and normalized before extracting proteasome-fractions and total protein amounts of these fractions were determined by Bradford assay and adjusted to equal amounts. Significance values were assigned using unpaired students T-Test. Note the significant decrease of proteasomal activity in cells overexpressing the p97 mutant. (B) In addition, immunoblotting of  $\beta$ -actin was performed as internal loading control (lower panel). Also shown is the p97 indirect immunoblotting of cell lysates.

#### 3.4.2. Defects in ERAD activity in the presence of mutated p97

The HMG-CoA reductase (HMGR) is the rate-limiting enzyme in cholesterol synthesis and thus is regulated to control cellular cholesterol levels. HMGR and other components of this pathway are regulated by the ERAD pathway. When cholesterol concentrations are low in a cell, HMGR is stabilized, because the mediator for its degradation, the ER resistant protein Insig-1 (insulin-induced gene 1), is degraded itself (Gong et al., 2006; Gong et al., 2006; Lee et al., 2006). The interaction of Insig-1 with HMGR (and Scap, see below) is sterol-dependent (Sun et al., 2005). For

HMGR stabilizing, Insig-1 is poly-ubiquitinated through the ubiquitin ligase gp78 (also named AMFR, autocrine motility factor receptor) in combination with p97 and subsequently directed to the proteasome for degradation (Gong et al., 2006; Lee et al., 2006). In addition, a complex of SREBP (sterol regulatory element-binding protein) and SCAP (SREBP-cleavage-activating protein) is formed and translocated to the Golgi, where proteolytic activation of SREBP occurs (Edwards et al., 2000; Goldstein et al., 2006). This translocation is driven by the interaction of the COPII coat proteins Sar1, Sec23 and Sec24 with SCAP/SREBP (Sun et al., 2005). Activated SREBPs can now induce expression of their target genes, including HMGR and Insig-1 (Edwards et al., 2000; Goldstein et al., 2006).

The interaction of these components changes, when cellular cholesterol levels are high. Now HMGR has to be degraded, which is induced by its poly-ubiquitination followed by proteasomal degradation. Interestingly, ubiquitination of HMGR is stimulated better by sterol intermediates like lanosterol (the first sterol intermediate in cholesterol synthesis) and other sterol-derivates than by cholesterol itself, which, in contrast, better stimulate the interaction of SREBPs (Song et al., 2005; Bengoechea-Alonso and Ericsson, 2007). Insig-1 has to mediate the interaction of gp78 and p97 with HMGR in a sterol-intermediate dependent manner (Song et al., 2005; Song et al., 2005). Also, the synthesis of HMGR has to be downregulated. This is done by retention of SCAP/SREBP in the ER through the formation of a stable complex of - once more - Insig-1 and SCAP/SREBP (Bengoechea-Alonso and Ericsson, 2007).

The involvement of p97 in cholesterol homeostasis and the finding of a putative binding pocket for a cholesterol like compound (see below) suggests a potential link

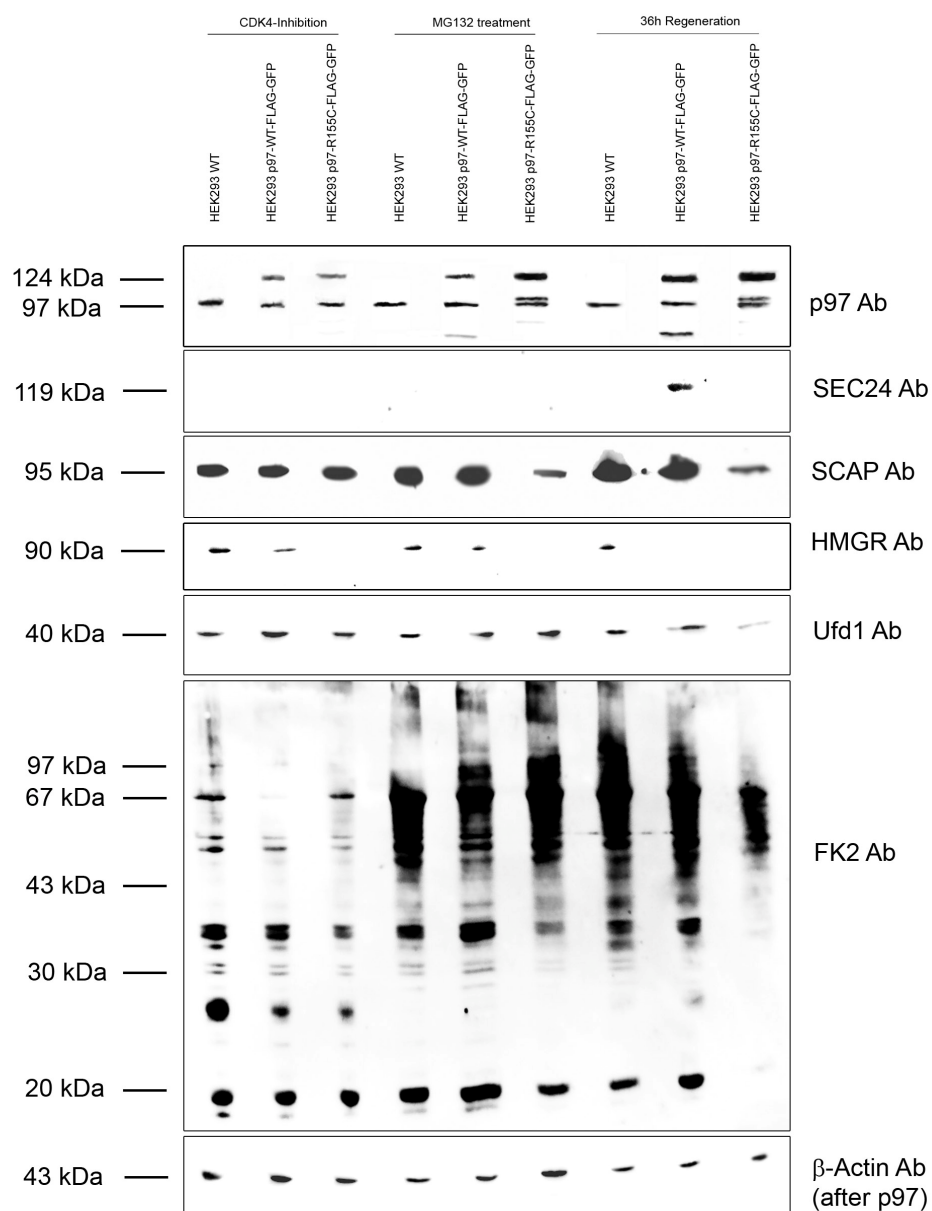
to a missregulated ERAD activity (Hübbers et al., 2007). Therefore we analyzed total cell lysates of HEK293 cells overexpressing wt-p97-FLAG-GFP and R155C-p97-FLAG-GFP along with untransfected HEK293 cells by immunoblotting with specific regard to selected compounds of the cholesterol homeostasis pathway. Lysates derived from untreated cells, from cells after 16 hours of incubation with the MG132 proteasome inhibitor, and after 36 hours of regeneration (the timepoint with the most significant difference in aggregate numbers, see chapter 3.3.2) were analyzed. Possible influences of different proliferation rates were ruled out by arresting the cell cycle in G1 phase while treating with a CDK4-Inhibitor. p97 immunoblotting revealed no significant differences in its signal intensities. However, bands corresponding to degraded p97 protein were detected consistently in stress experiments (Fig. 23). The protein expression level of the p97 interacting protein Ufd1 was significantly decreased in cells overexpressing the R155C-p97 mutant. Furthermore, staining for poly-ubiquitin showed significant differences for R155C-p97-FLAG-GFP compared to the untransfected and wt-p97-FLAG-GFP overexpressing cells. These differences are obvious throughout the whole experiment and predominantly affected the total pattern of poly-ubiquitination 36 h after removal of MG132. HMG-CoA reductase is equally expressed for untransfected cells in all cases analysed. Wt-p97-FLAG-GFP overexpressing cells showed a HMGR signal similar in intensity compared to the untransfected cells, but the signal disappears 36 h after MG132 removal. Strikingly, the HMGR signal is absent for R155C-p97-FLAG-GFP overexpressing cells throughout the whole experiment. The COPII coat protein Sec24 is solely expressed in wt-p97-FLAG-GFP overexpressing cells 36 h after MG132 removal. SCAP showed a decrease in signal intensity for

R155C-p97-FLAG-GFP overexpressing cells after aggregate induction by MG132 treatment and during regeneration.

The cholesterol level regulating pathway is an example where several components are specifically degraded through ERAD with p97 being a central component of the latter (Goldstein et al., 2006). Mutated p97 may exert a specific defect in interaction with one or more component(s) of this pathway and thus disrupting this specific ERAD function.

***Fig. 23. (Page 46) Western blot analysis of p97 and several ERAD and cholesterol homeostasis pathway associated proteins.***

*Total protein extracts from non-transfected and transfected HEK293 cells overexpressing wt-p97-FLAG-GFP and R155C-p97-FLAG-GFP were loaded for Western blotting as indicated. Cells were treated with CDK4 throughout the experiment. Cell lysates were analyzed directly after CDK4 treatment, 16 h after MG132 incubation and 36 h after removal of MG132. p97 shows degraded protein bands for both overexpressing cell lines under stress conditions. HMG-CoA reductase is absent in mutant p97 overexpressing cells at both timepoints and SCAP is downregulated for mutant p97 under stress conditions. Ufd1 levels were equal at all times but decreased for mutant p97 during regeneration. Sec24 showed a single band for wt-p97-FLAG-GFP during regeneration. The pattern of poly-ubiquitinated proteins is modified for mutant p97.  $\beta$ -Actin stainings were used as internal loading controls (lower panel; after p97 blot; loading controls of other blots not shown).*



### 3.4.3. Fluorescence protease protection assay analysis of ER and Golgi morphology

To elucidate possible morphological changes of the ER and Golgi structures due to mutant p97 or any changes in localization of wt and mutant p97 at these organelles, we performed a fluorescence protease protection (FPP) assay (Lorenz et al., 2006).

We therefore co-transfected marker proteins into our stably transfected HEK293 cells overexpressing wt-p97-FLAG-GFP and R155C-p97-FLAG-GFP. For ER staining we used pDsRed2-ER vector (Clontech No. 632409), which uses the ER targeting sequence of calreticulin fused N-terminally to the fluorochrome as well as the KDL ER retention sequence at the C-terminus of the fluorochrome. As a Golgi marker we used pDsRed-Monomer-Golgi (Clontech No. 632480), which uses the N-terminal 81 amino acids of human beta-1,4-galactosyltransferase comprising the membrane anchoring signal peptide of 1,4-GT fused to a C-terminal fluorochrome. The fusion protein is therefore directed to the transmedial region of the Golgi apparatus.

24 hours after transfection, both ER- and Golgi-markers showed an intense labeling and a typical distribution for these organelles with no differences between wt and mutant p97 (Fig. 24E, F, K, L, Q, R and Fig. 25E, F, K, L, Q, R). Thus, to remove free cytoplasmic p97-GFP and to demask possible differences in the enrichment of p97-GFP in these organelles, we incubated cells with 20  $\mu$ M digitonin for 1 minute followed by 4 mM trypsin for 5 minutes. The fluorescence signals of the ER and Golgi markers which were not affected by this treatment were compared to the remaining non-cytoplasmic p97 signals. The Golgi marker did not present a co-localization with p97 (Fig. 24O and U) while the ER marker exhibited a partial co-localization with p97, however, without differences between wt- and R155C-p97 (Fig. 25O and U). Expression of the mutant p97 did not change the morphology of the ER or Golgi apparatus.

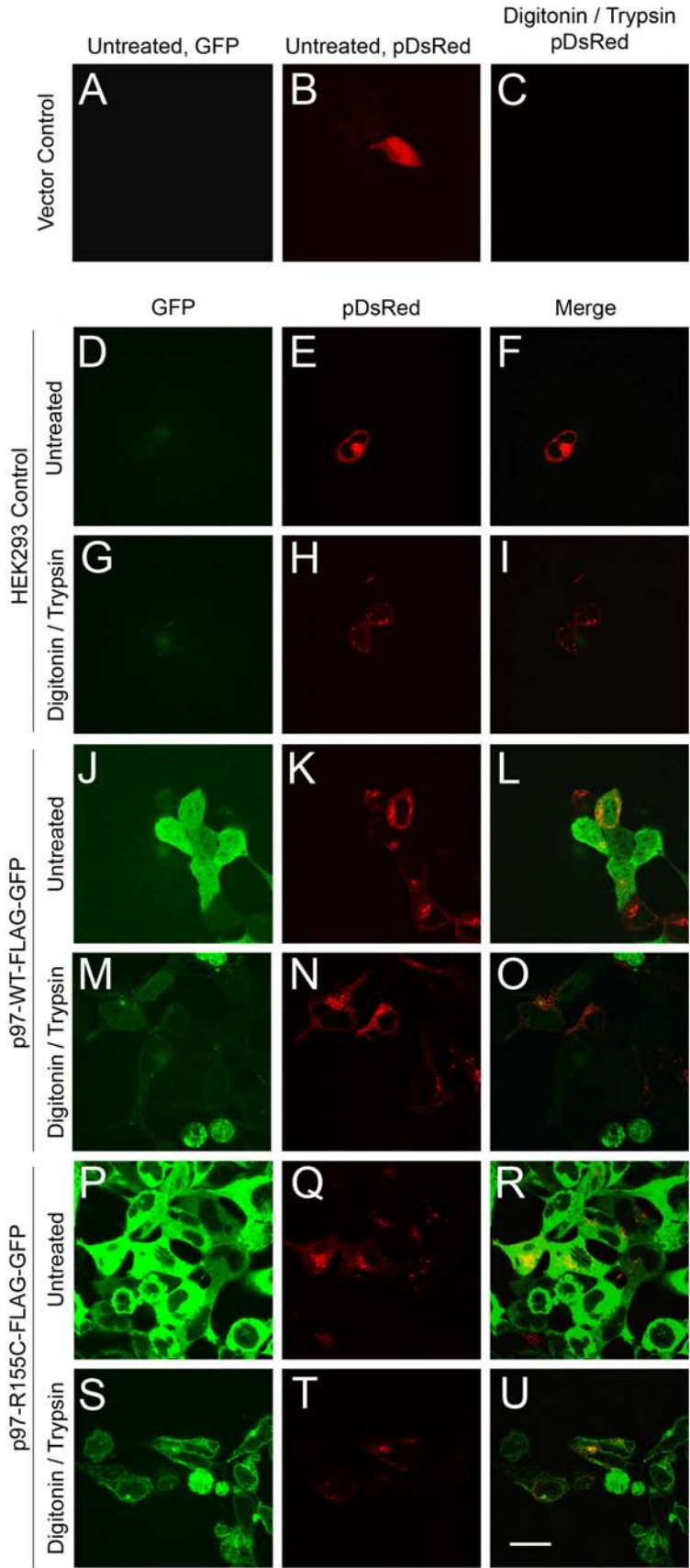
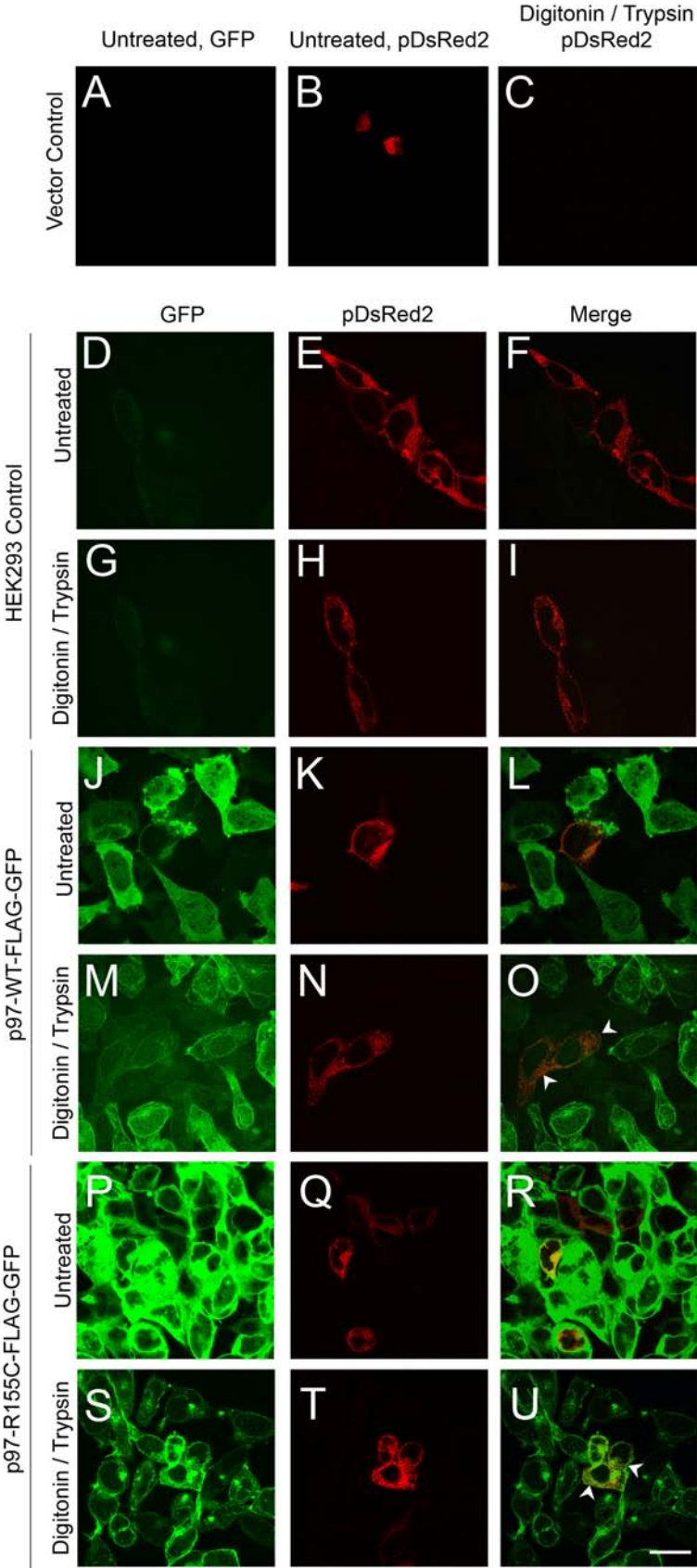


**Fig. 24. (Page 48) Fluorescence protease protection assay of the Golgi apparatus.** Confocal images of HEK293 cells stably overexpressing wt- or R155C-p97-FLAG-GFP protein. In addition, a Golgi marker fused to an N-terminal pDsRed-Monomer vector was transiently transfected. All cells were fixed using paraformaldehyde. Treated cells were incubated with 20  $\mu$ M digitonin for 1 minute followed by 4 mM trypsin for 5 minutes before fixation. (A – C) Empty vector control, (A) GFP signal, (B) vector signal, (C) vector after digitonin / trypsin incubation followed by fixation. (D – I) p97 untransfected HEK293 cells transiently expressing Golgi marker. (D – F) fixation only, (G – I) after digitonin / trypsin treatment. (D, G) GFP signal, (E, H) Golgi marker, (F, I) merge. (J – O) cells stably overexpressing wt-p97-FLAG-GFP and transiently pDsRed-Monomer-Golgi, (J – L) fixation only, (M – O) digitonin / trypsin incubation. (J, M) wt-p97, (K, N) Golgi marker, (L, O) merge. (P – U) cells stably overexpressing R155C-p97-FLAG-GFP and transiently pDsRed-Monomer-Golgi, (P – R) fixation only, (S – U) fixation after digitonin / trypsin incubation. (P, S) R155C-p97, (Q, T) Golgi marker, (R, U) merge. Bar, 20  $\mu$ M.

**Fig. 25. (Page 50) Fluorescence protease protection assay of the Endoplasmic reticulum**

Confocal images of HEK293 cells stably overexpressing wt- or R155C-p97-FLAG-GFP protein. In addition, an ER marker fused to an N-terminal pDsRed2 vector was transiently transfected. All cells were fixed using paraformaldehyde. Treated cells were incubated with 20  $\mu$ M digitonin for 1 minute followed by 4 mM trypsin for 5 minutes before fixation.

(A – C) Empty vector control, (A) GFP signal, (B) vector signal, (C) vector after digitonin / trypsin incubation followed by fixation. (D – I) p97 untransfected HEK293 cells transiently expressing ER marker. (D – F) fixation only, (G – I) after digitonin / trypsin treatment. (D, G) GFP signal, (E, H) ER marker, (F, I) merge. (J – O) cells stably overexpressing wt-p97-FLAG-GFP and transiently pDsRed-ER, (J – L) fixation only, (M – O) digitonin / trypsin incubation. (J, M) wt-p97, (K, N) ER marker, (L, O) merge. (P – U) cells stably overexpressing R155C-p97-FLAG-GFP and transiently pDsRed-ER, (P – R) fixation only, (S – U) fixation after digitonin / trypsin incubation. (P, S) p97-R155C, (Q, T) ER marker, (R, U) merge. Colocalizing p97 and ER-marker is indicated by arrowheads in the merges, respectively. Bar, 20  $\mu$ M.



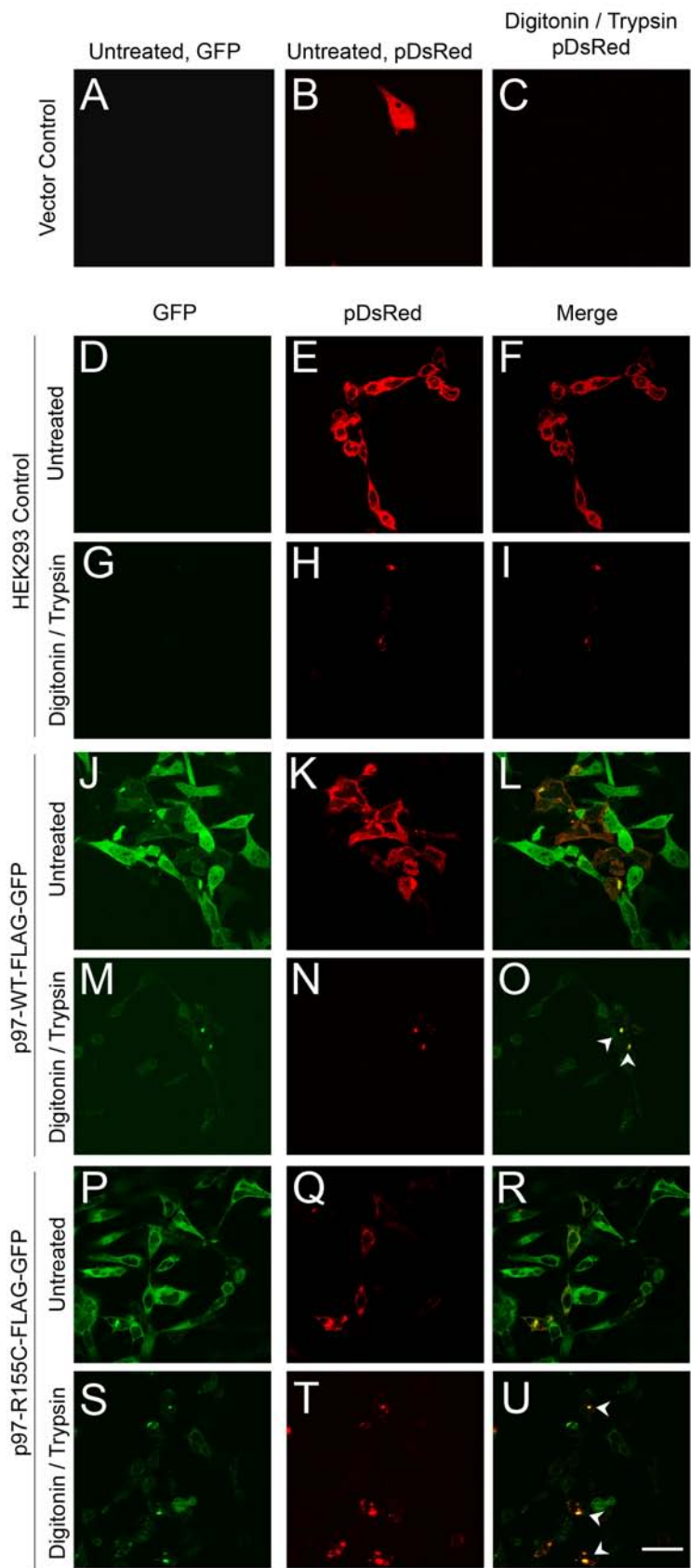
#### 3.4.4. *Fluorescence protease protection assay of autophagosomes*

The two major cellular protein degradation systems, the ubiquitin-proteasome system and the autophagy machinery are functionally coupled (Ding et al., 2007; Pandey et al., 2007). Downregulation of UPS results in an upregulation of autophagy. We therefore analyzed autophagic activity in our wt and mutant p97 overexpressing HEK293 cells. GAPDH (Glyceraldehyde-3-phosphate dehydrogenase) is established as a marker for autophagosomes (Lorenz et al., 2006). GAPDH is an ubiquitously and strongly expressed cytosolic protein, which is randomly degraded through autophagy as many other proteins, too, and thus can be used as a marker for autophagic vacuoles. We used the GAPDH sequence of a commercially available GAPDH-CFP vector (GeneCopoeia, USA) and cloned it C-terminally to a pDsRed2 vector.

Both untransfected and wt-p97-FLAG-GFP overexpressing HEK293 cells showed a strong cytoplasmic staining for GAPDH (Fig. 26E and K). After treatment with digitonin and trypsin almost all GAPDH is washed out of the cell (Fig. 26H and N). The remaining spots of GAPDH perfectly colocalize with spots in the wt-p97 signal (Fig. 26N). R155C—p97-FLAG-GFP overexpressing HEK293 cells on the other hand show a less intense GAPDH signal compared to the wt situation in untreated cells. Digitonin and trypsin treatment at least unmasks a marked increase in remaining GAPDH spots, which also colocalise with the p97 signal. This finding indicates an upregulation of autophagy in mutated p97. We therefore can conclude that significant downregulation of proteasomal activity in R155C mutant HEK293 cells also results in a predicted upregulation of autophagy. The decreased amount of cytosolic GAPDH therefore could well be a result of an increased overturn of

cytosolic proteins. The colocalisation of p97 with the autophagosomes implicates two possibilities. On the one hand p97 could simply be degraded by the autophagosomes. On the other hand p97 has a functional role in the autophagy pathway. This issue has to be further investigated.

**Fig. 26. (Page 53) Fluorescence protease protection assay of autophagosomes**  
Confocal images of HEK293 cells stably overexpressing wt- or R155C-p97-FLAG-GFP protein. In addition, GAPDH fused to an N-terminal pDsRed2 vector was transiently transfected. All cells were fixed using paraformaldehyde. Treated cells were incubated with 20  $\mu$ M digitonin for 1 minute followed by 4 mM trypsin for 5 minutes before fixation.  
(A – C) Empty vector control, (A) GFP signal, (B) vector signal, (C) vector after digitonin / trypsin incubation followed by fixation. (D – I) p97 untransfected HEK293 cells transiently expressing GAPDH marker. (D – F) fixation only, (G – I) after digitonin / trypsin treatment. (D, G) GFP signal, (E, H) GAPDH marker, (F, I) merge. (J – O) cells stably overexpressing wt-p97-FLAG-GFP and transiently pDsRed-GAPDH, (J – L) fixation only, (M – O) digitonin / trypsin incubation. (J, M) p97-wt, (K, N) GAPDH marker, (L, O) merge. (P – U) cells stably overexpressing R155C-p97-FLAG-GFP and transiently pDsRed-GAPDH, (P – R) fixation only, (S – U) fixation after digitonin / trypsin incubation. (P, S) p97-R155C, (Q, T) GAPDH marker, (R, U) merge. Arrowheads shown in the merges mark partial colocalization of p97 and GAPDH, respectively. Bar, 20  $\mu$ M.



### 3.5. Filter assay combined with GC/MS analysis of putative ligands binding to recombinant p97

In collaboration with A. Hofmann (Brisbane, Australia) we studied wt and mutated p97 in an *in silico* approach (Hübbers et al., 2007). Therefore the R93C, R155H and R155C mutations were introduced into a human p97 protein model derived from the murine p97 crystal structure. Analysis indicates that R93 and R155 are surface-accessible residues located in the center of cavities that may enable ligand binding in both the monomeric as well as the hexameric state of p97. These cavities may be putative ligand-binding sites. To find potential ligands for the two putative R93 and R155 ligand-binding pockets, the automated docking programme LIDAEUS was used to screen a small-molecule database for potential ligands. For the R155C cavity, a steroid (16 $\alpha$ -hydroxypregnenolone; Sigma H8252; SPH1-005-061) as well as a hexose-like compound (N-acetyl- $\alpha$ -D glucosamine-1-phosphate disodium salt; Sigma A2142;SPH1-000-376) could be identified. For the R93 pocket screening resulted in the cyclic sugars  $\alpha$ -D-glucose-1-phosphate disodium salt (Sigma G7000; SPH1-004-510) and  $\alpha$ -D-galacturonic acid-1-phosphate lithium salt (Sigma G4884; SPH1-004-402).

To verify a binding of these ligands, we performed a filter assay with purified recombinant p97-wt, p97-R93C, p97-R155C and p97-R155H. Since an interaction of p97 with the cholesterol homeostasis pathway is well established and many components in this pathway interact in a sterol-dependent manner, we first focused on the cholesterol derivate 16 $\alpha$ -Hydroxypregnenolone as well as the structurally closely related 25-Hydroxycholesterol. Therefore we incubated the recombinant

proteins with 100x molar excess of the cholesterols. After removal of unbound cholesterol molecules by centrifugation through a Millipore Ultrafree-MC NMWL 10.000 Biomax 10 filter (Millipore, Germany), ligands that may have bound to the recombinant p97 should be immobilized on the membrane. Bound ligands were eluted with 0,1% trifluoro acetic acid (TFA) in PBS. In collaboration with another group in our institute (F. G. Hanisch) the potential ligands were analysed by gas chromatography coupled to mass spectrometry. Unfortunately, none of the both ligands was detected to bind to the recombinant p97. Although this GC/MS method is extremely sensitive (femtomolar concentrations can be detected), ligands with low affinity to p97 may not be detected. As our structural analysis indicated, the formation of p97 homohexamers is important for ligand binding. This hexamerisation was intensively studied for p97-wt and p97-R155H by Wehl et al. (2006) and the hexamers are reported to elute exclusively from a size exclusion column for both recombinant wt and mutant p97. Thus, the absence of the compounds in our analysis could be more due to a weak interaction of p97 and its ligands than due to a disrupted homohexamere formation. We therefore plan to test possible interactions employing isothermal calorimetry.

### **3.6. Generation of a R155C-p97 mouse knock-in targeting vector**

Further investigations of human IBMPFD tissue are restrained by the very limited amount of biopsy material available. Furthermore, this biopsy material mostly reflects very late stages of the progressive pathology. Genetic mouse models are powerful tools for investigating a disease relevant protein in the context of a complex organism and throughout all stages of the disease. Thus, we decided to generate a

R155C-p97 knock-in mouse. The particular R155C mutation was chosen because it showed the most severe phenotype in patients.

The murine p97 gene is located on chromosome 4 and consists of 17 exons spanning over approximately 30 kb. Murine and human p97 proteins share 99.5% identity with Ile206 being Val in the mouse protein. Residue R155 is coded by the first bases of exon 5. The homology arms of the targeting vector and the cDNA fragments to be used as southern probes have been amplified by PCR using BAC-clones RPCI23-124L1 and RPCI24-186I11 as templates. The R155C-p97 mutation was introduced by *in vitro* mutagenesis. The targeting vector was verified by restriction digestion and sequencing (data not shown), the southern probes have been tested with wild type ES-cell DNA (data not shown).

Figure 27 demonstrates a simplified scheme indicating important aspects of the targeting vector, targeting locus, and restriction enzymes and fragments for the identification of homologous recombination. The resistance cassette for selection of positive ES-cell clones is positioned between exons 4 and 5 without disturbing conserved intron structures. The neomycin resistance is flanked by loxP sites allowing its deletion by a transient expression of Cre-recombinase. Neomycin gene and flanking loxP-sites have the same orientation as the p97 gene. Removal of the neomycin cassette preserves the original length and structure of the p97-mRNA. This targeting strategy of the murine genome leads to a genetic state with one wild type and one mutated p97 allele as identified in human IBMPFD patients. The R155C-p97 knock-in vector will be used for the generation of the first p97 knock-in mouse available subsequent to this work.

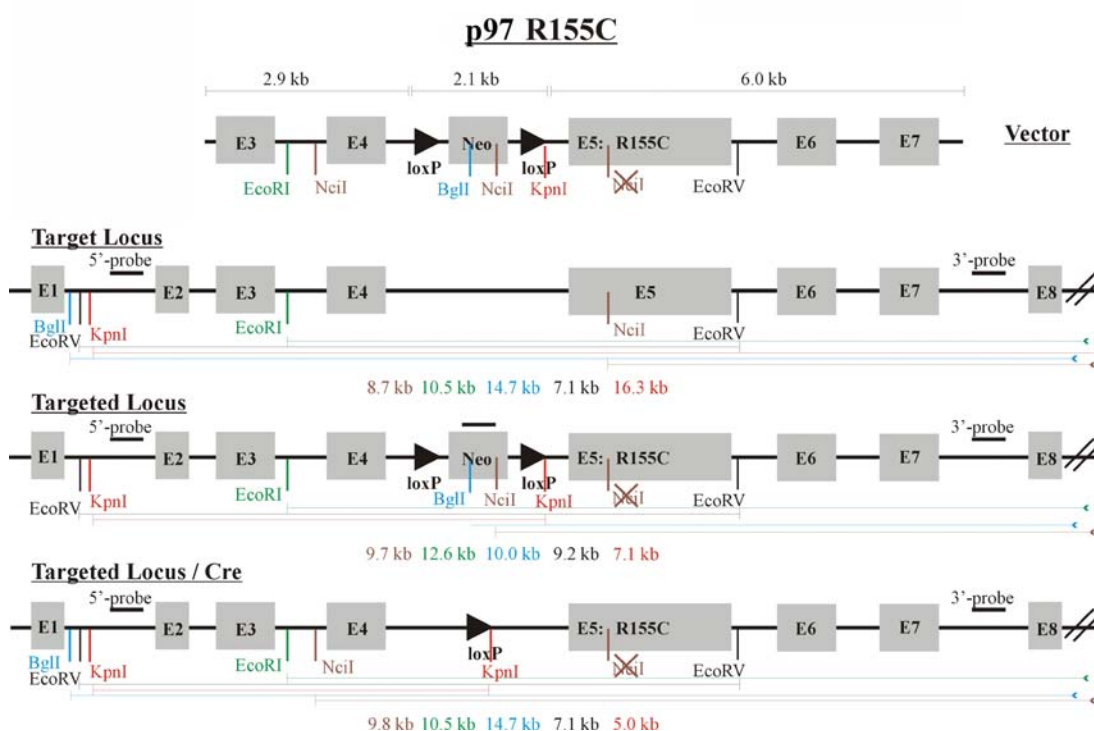


**Fig. 27. Scheme of the R155C-p97-targeting vector and the targeted p97 gene locus.**

The p97 intron sequence between exons 4 and 5 was replaced by the neomycin resistance gene (neo) flanked by two loxP-sites. The location of the 5' and 3' probes for Southern blot analysis are indicated. For the 5' probe, upon KpnI digestion the wild type and deleted allele yield fragments of 16,3 and 7,1 kb, respectively; upon EcoRV digestion the wild type and deleted allele yield fragments of 7,1 and 9,2 kb, respectively. For the 3' probe, upon EcoRI digestion the wild type and deleted allele yield fragments of 10,5 and 12,6 kb, respectively; upon EcoRI digestion the wild type and deleted allele yield fragments of 14,7 and 10 kb, respectively, and upon NciI digestion the wild type and deleted allele yield fragments of 18,7 and 9,7 kb, respectively.

## **4. Discussion**

### **4.1. Clinical phenotype**

Our histopathological analysis revealed a broad spectrum of pathological changes in muscle reflecting different stages of disease progression in our three IBMPFD patients. Immunostaining using p97 antibodies demonstrated the presence of p97-positive cytoplasmic aggregates, a phenomenon previously described (Watts et al., 2004). Our analysis demonstrated that these p97-positive aggregates also display positive ubiquitin staining. As a further novel finding we demonstrated the presence of p97- and ubiquitin-positive nuclear inclusions in muscle. This aspect mirrors the brain pathology in IBMPFD, which is characterized by the presence of p97- and ubiquitin-positive nuclear inclusions in neurons (Schröder et al., 2005). Our ultrastructural analysis demonstrated that both the cytoplasmic and the nuclear inclusions in IBMPFD muscle were composed of haphazardly arranged filaments. In analogy to the aberrant desmin immunofluorescence staining, our ultrastructural studies revealed the presence of desmin-positive granulofilamentous material, the characteristic ultrastructural hallmark of primary desminopathies and myofibrillar myopathies (Schröder et al., 2003; Selcen et al., 2004; Bär et al. 2005). This finding indicates that, at least in advanced degenerative stages of IBMPFD, p97 mutations induce secondary alterations of the extrasarcomeric desmin cytoskeleton.

The post-mortem analysis of patient II revealed a novel clinical aspect in IBMPFD. p97 mutations not only affect skeletal muscle, but may also lead to a dilatative cardiomyopathy characterized by ubiquitin-positive cytoplasmic aggregates and nuclear inclusions.

#### 4.2. Analysis of the p97 protein expression and localization

Our immunoblotting analyses revealed no significant differences in the total amount, subcellular distribution and posttranslational modifications of p97 protein between normal and diseased muscle. In contrast to IBMPFD muscle, where endogenous p97 is solely present in the insoluble fraction, western blot analysis of transfected cells (wt- and mutant-p97) demonstrated that endogenous and transfected p97 is predominately present in the soluble protein fraction.

Neither morphology nor p97 distribution were affected in our cell culture experiments using primary myoblasts derived from patient muscle biopsy and HEK293 and C2F3 cells overexpressing wt or mutant p97. In addition we performed functional studies on these cells. Overexpression of p97 in HEK293 and C2F3 cells reduced proliferation rates, however without any difference between wt and mutant p97, as it has been reported earlier (Zhang et al., 1999). In contrast to IBMPFD-muscle, all our transient and stable transfection experiments using mutant- and wt-p97 did not lead to cytoplasmic or nuclear protein aggregate formation. Only treatment of HEK293 cells with the proteasome inhibitor MG132 led to the formation of pathological protein aggregates. Aggresome formation by proteasome inhibitors in HEK293 cells have previously been described by Meriin et al. (1998). Again, no apparent differences in the extent or subcellular localization of the protein aggregates could be detected. Various other cell stress experiments like treatment with mitomycin C, UV radiation, H<sub>2</sub>O<sub>2</sub>, osmotic shock, wortmannin, and *clasto*-lactacystin  $\beta$ -lactone as well as the use of differentiated C2F3 myotubes did not provide evidence for abnormal protein aggregate formation.

These findings are in contrast to the recently published study by Weihl et al. (2006), who described large perinuclear aggregates in up to 33% of cells transfected with R155H-p97-GFP and R95G-p97-GFP, and in 7% of cells transfected with wt-p97-GFP. These aggregates were reported to contain poly-ubiquitinated proteins, a subgroup also mutated p97 protein. A potential cause for aggregates in such transient transfection experiments may be strong overexpression of the transfected gene. This is strongly supported by the following reasons: i) A previous study by Ye et al. (2004) demonstrated strikingly similar perinuclear aggregates in double transient transfection studies using His-wt-p97 and Myc-wt-VIMP, a membrane protein that recruits the p97-ATPase. ii) In our immunoblot-controlled stable transfections a ratio of 1:3 of mutant-p97 to wt-p97 did not lead to protein aggregate formation. iii) In primary human myoblasts derived from IBMPFD skeletal muscle, which most closely represent the physiological situation with one wt and one mutated p97 allele, no abnormal protein aggregation was detected by p97 and FK2 immunostaining. iv) In the vast majority of IBMPFD patients, it takes at least 40 to 50 years until the disease manifests and protein aggregates are exclusively found in post-mitotic cells (neurons, striated muscle cells).

#### **4.3. Structural analysis of wild type p97 versus R93 and R155 mutant p97**

All three p97 mutations identified in our IBMPFD patients concern evolutionarily highly conserved arginine residues in the CDC48 domain of the p97 protein (Fig. 1). In the light of a previous study showing that p97 mutations impair ERAD (Weihl et al. 2006), the binding of recombinant p97 to various ERAD-p97-co-factors and other known ligands was studied in collaboration with A. Böddrich (Berlin) (Hübbers et

al., 2007). The GST pull-down assays demonstrated that wt-p97 as well as all three p97 mutants showed identical binding to Ufd1- (Fig. 28), Npl4- and ataxin-3 (data not shown).

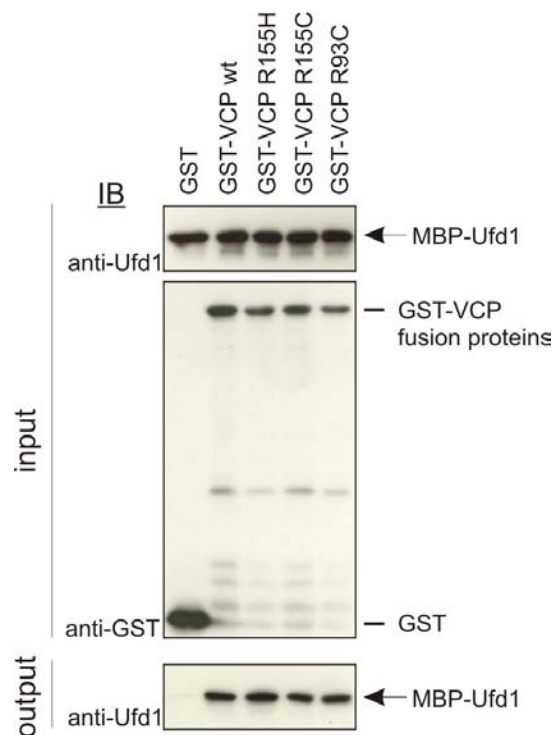


**Fig. 28. GST pull-down experiments with purified MBP-Ufd1.**

*GST-p97 fusion proteins were bound to glutathione agarose beads and incubated with MBP-Ufd1. After extensive washing of the beads, bound protein was detected by immunoblotting using an anti-Ufd1 antibody (bottom panel). Ten per cent of the input binding mixture was subjected to immunoblot analysis with anti-Ufd1 (top panel) and anti-GST antibody (middle panel). (Hübbers et al., 2007)*

With regard to protein aggregate formation, it was tested whether purified wild type and mutant p97 can form SDS-insoluble aggregates *in vitro* using a filter retardation assay (Wanker et al., 1999). These experiments showed that neither mutant p97 nor wild type p97 formed SDS-insoluble aggregates *in vitro* (Hübbers et al., 2007). Furthermore, in a previous study, the ATPase-activity of purified R155H-p97 was similar to the one reported for wt-p97 (Weihl et al., 2006). These results imply that

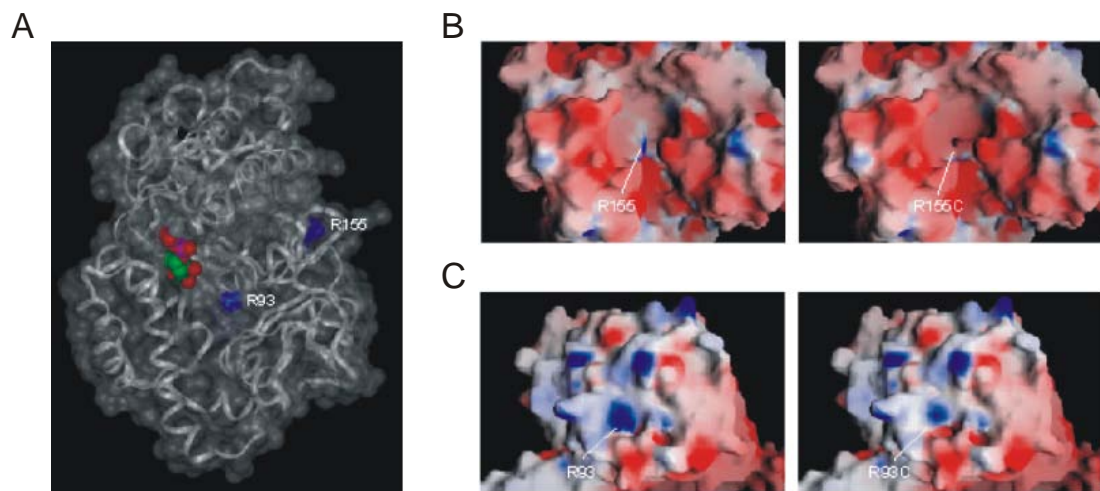
the various p97 mutants analyzed so far are not associated with gross alterations in p97 binding to known cofactors and its intrinsic ATPase enzyme activity. This favors the hypothesis that IBMPPFD pathology is due to a toxic gain of p97 function.

To address the pathological consequences of p97 mutations at the structural level, the R93C, R155H and R155C mutations were introduced into a human p97 protein model derived from the murine p97 crystal structure, done in collaboration with A. Hofman (Hübbers et al., 2007). The analysis indicates that R93 and R155 are surface-accessible residues located in the center of cavities that may enable ligand binding (Fig 29). Both R93 and R155 are also surface accessible in the hexameric state of p97 (data not shown).

While the cleft around R155 is larger and predominantly negatively charged (Fig. 29B), the cavity around R93 appears smaller and rather positively charged (Fig. 29C). The particular shape and charge distribution within the clefts around R93 and R155 indicate that these may be putative ligand-binding sites.

***Fig. 29. (Page 63) Transparent Connolly surface with ribbon backbone of the human p97 model.***

*The bound ADP in the D1-nucleotide-binding site is shown as Corey, Pauling, Koltun colouring scheme. The locations of the clefts around R93 and R155 are indicated by blue coloring of the surface of the two arginine residues; prepared with InsightII. (C and D) GRASP (Nicholls et al., 1993) surface representations coloured by electrostatic surface potential (red: negative, blue: positive). Shown are the clefts around R155 (C), as well as R93 (D). Wt R155 and R93 are represented on the left, while mutant R155C and R93C are shown on the right (Hübbers et al., 2007).*



Further analysis revealed that R93 maintains interactions with amino acid residues E194 and R65, as well as with the backbone carbonyl group of N90. These interactions are all within the cleft around R93. The R93C mutation leads to a loss of these contacts due to the shorter side chain of cysteine.

In contrast, R155 interacts with amino acid residue N387 residing in the D1-domain, which binds and hydrolyses ATP. The N- and D1-domains are spatially separated and form only three direct contacts, R155-N387, R89-E261 and E30K217. The mutations R155C and R155H lack the interaction with N387 owing to the shorter amino acid side chains and thus may alter the relative orientation of the N- and D1-domains of p97.

DeLaBarre and Brünger (2003) proposed a model where the mobile state of the N-domain is triggered by release of a latch provided by the D1 $\alpha$ -domain. Three pairs of residues can be identified that could act as latch. Importantly, one of these pairs is R155-N387. A p97 mutant with an impaired ability to lock the N-domain is very likely to have lost its regulatory properties. R93 maintains interactions with amino acid residues E194 and R65, as well as with the backbone carbonyl group of N90.

The R93C mutation leads to a loss of these contacts due to the shorter side chain of cystein.

#### 4.3.1. *In silico screening of small ligand binding*

Since our biochemical analysis did not reveal any detectable changes in the binding of wt-p97 versus mutant-p97 to known p97 ligands, a small-molecule database was screened in collaboration with A. Hofman for potential ligands for the two putative R93 and R155 ligand-binding pockets using the automated docking programme LIDAEUS (Hübbers et al., 2007). LIDAEUS generates sitepoints in the binding pockets and aims to find and dock ligands matching the pockets by chemical and shape complementation. The conformations are ranked according to various energy scores including hydrophobic interactions, and van der Waals and H-bonding (Wu et al., 2003). From the database comprising around 10,000 molecules, interesting ligands were picked for further analysis based on visual screening of the fit to the pocket and the LIDAEUS scoring.

The negatively charged R155 site is located at the interface between the N- and D1-domains. The virtual screening approach considering docking and chemical interaction indicated that ADP/ATP are unlikely binding partners for the R155 site, but identified a steroid (16 $\alpha$ -hydroxypregnenolone; Sigma H8252; SPH1-005-061) as well as a hexose-like compound (N-acetyl- $\alpha$ -D-glucosamine-1-phosphate disodium salt; Sigma A2142; SPH1-000-376) as ligands with significantly higher binding scores than all other target screened compounds (Fig. 30A).

Although the R155 pocket is not a typical steroid binding pocket (Tanenbaum et al., 1998; Williams and Sigler, 1998; Bledsoe et al., 2002; Li et al., 2005), some of the

p97:SPH1-005-061 interacting residues are analogous to the amino acid–steroid contacts made by the steroid receptors.

The R93 pocket is composed of residues from the N-D1-linker region and some residues from the surface of the N-domain. The amino acid residues of the linker region constitute the top of the pocket. Thus, movement of the linker would not destroy the binding site, but make it more flexible. LIDAEUS screening yielded a number of putative target molecules. The highest scoring compounds were the cyclic sugars ( $\alpha$ -D-glucose-1-phosphate disodium salt; Sigma G7000; SPH1-004-510 and  $\alpha$ -D-galacturonic acid-1-phosphate lithium salt; Sigma G4884; SPH1-004-402) (Fig. 30B).

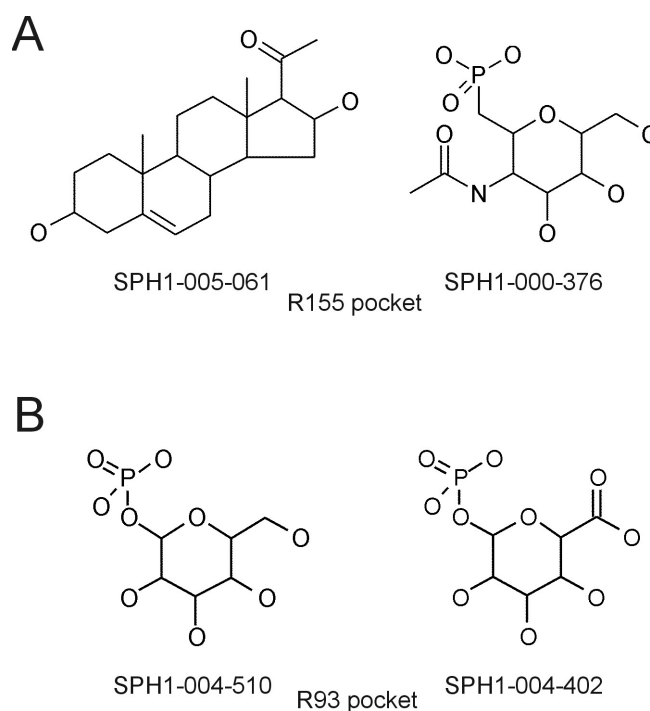


**Fig. 30. Selected putative lead compounds suggested by LIDAEUS and confirmed by visual inspection of the docked ligands in the R155 (A) and R93 (B) pocket.**

The appearance of sugar-like and cholesterol like compounds for the R93 and R155 sites establishes a link to the reported interactions between p97 and SCF<sup>(Fbs1,2)</sup>, a cytosolic ubiquitinase for glycoproteins and gp78 (also named AMFR, autocrine motility factor receptor), an ER membrane resistant ubiquitin ligase and deglycosidase (Fang et al., 2001; Ye et al., 2005; Yoshida et al., 2005). Furthermore, p97 is reported to control N-glycosylation in the ER (Lass et al., 2007). Interestingly, mutation of UDP-N-acetylglucosamin 2-epimerase/N-acetylmannosaminase is reported to causes IBM (Eisenberg et al., 2001; Kayashima et al. 2002). Here, it is tempting to speculate that p97 mutations interfere with the binding to carbohydrates from misfolded glycoproteins in the endoplasmic reticulum and cytosol and with cholesterol derivatives (Spiro, 2002; Goldstein et al., 2006; Hübbers et al., 2007).

#### **4.4. Analysis of proteasome and ERAD activity**

As the R155C-p97 mutation showed the most severe phenotype in our patients, we focused on this mutation. Having demonstrated that MG132-dependent inhibition of the proteasomal activity leads to the formation of similar amounts of protein aggregates in HEK293 cells overexpressing wt- and R155C-p97-FLAG-GFP, we analyzed the progression of the aggregates in the course of further cultivation of these cells. Interestingly, HEK293 cells overexpressing R155C mutant p97 exhibited significant delay in the rates in clearing the protein aggregates. After extended time, however, HEK293 cells overexpressing the mutant p97 also reduced the number of protein aggregates to levels found in the wt control.

#### 4.5. Role of p97 in the regulatory ERAD pathway

Immunoblotting of total cell lysates from untransfected and wt-p97 and R155C-p97 transfected HEK293 cells under non-stressed and MG132 stressed conditions showed that i) the poly-ubiquitination of proteins seem to be disturbed in R155C mutated p97. ii) The protein expression of Ufd1 appears to be reduced in mutant p97. iii) HMG-CoA reductase being not detectable in the case of mutated p97 could be explained by either a defect in its stabilization, or due to lack in the induction of its transcription. iv) The second hypothesis can be underlined by the findings that the COPII coat protein Sec24 also was not detected in R155C mutated p97 which leads to a defect in the translocation of the complex composed of SREBP (sterol regulatory element-binding protein) and SCAP (SREBP-cleavage-activating protein) and thus their activation in the GOLGI, and finally the observation that v) SCAP was found downregulated in these mutated cells under stress conditions.

Some of the proteins involved in this pathway are selectively driven to proteasomal degradation via the ERAD pathway, which is done through poly-ubiquitination followed by processing to the proteasome, or are protected against degradation via selective binding to poly-ubiquitination inhibiting compounds. For many of the protein-protein interactions in this regulatory pathway cholesterol and cholesterol like compounds were identified as mediators for their binding (Song et al., 2005; Sun et al., 2005; Bengoechea-Alonso and Ericsson, 2007). Our *in silico* findings showed a putative interaction of p97 with a sterol compound which may be disrupted by the R155 mutations. For the R155C mutated p97 we could show that components of the sterol dependent HMGR homeostasis pathway and HMGR itself are significantly missregulated. Thus, it is not unlikely to speculate that a sterol dependent complex

formation of p97 and other components is disturbed. Finally, this would lead to a disrupted ERAD function and degradation-prone proteins could accumulate.

These findings are underlined by our analysis of the proteasomal activity. HEK293 cell extracts enriched in proteasomes were used to quantify the proteasomal activity. Here, overexpression of p97 increased the proteasomal activity compared to non-transfected HEK293 cells. In contrast, cells overexpressing R155C mutated p97 indicated a marked inhibition of all three major proteasomal activities. In a recent study, Kobayashi et al. (2007) report on p97 being involved in the re-solubilisation process of abnormal protein aggregates. Thus, the protein aggregates induced by MG132 treatment may be accessible for degradation in both wt and mutated p97 overexpressing cells. However, the marked delay in the aggregate clearance of cells overexpressing p97 mutant protein may be attributed to a disturbed proteasomal function. In line with reports indicating a close relation of proteasomal activity and autophagy, our findings further indicate that the downregulation of proteasomal activity is coupled to an upregulation of autophagic processes in IBMPFD (Brodsky and Scott, 2007; Ding et al., 2007; Pandey et al., 2007; Rubinsztein, 2007).

#### **4.6. Outlook**

In the field of known p97 cofactors, there should be a good chance to find additional pathways where mutated p97 is involved. Therefore, GST *pull down* experiments with special emphasis on the differences between wt- and mutated p97 protein will be performed together with total cell lysates of cultured cells and with patient

material. In addition, these *pull down* experiments should be performed in the presence of the putative small molecule ligands found in our *in silico* analysis.

To analyse the interaction of p97 with these potential ligands, as an alternative assay to gas chromatography coupled to mass spectrometry, isothermal calorimetry will be performed.

Furthermore, the morphological and biochemical characterization of the sequential steps of the progressive IBMPFD muscle pathology should be analyzed in more detail. Therefore a p97 R155C knock-in mouse model is in progress. Here, special emphasis should be placed on the comparison of pathological findings in human and murine IBMPFD muscle tissue, too.

The effects of the R155C-VCP mutant on the ubiquitin proteasome pathway shown in this work will be further analyzed in other cell culture models and in material from biopsy of human IBMPFD muscle and, once it is available, in mouse muscle.

RNA-microarray and proteome analysis of IBMPFD muscle tissue derived from early disease stages may underline - beside other new findings - our results in the missregulated HMG-CoA reductase pathway. Some interesting components in this pathway, especially the ubiquitin ligase and deglycosidase gp78, are interesting compounds where a cholesterol-mediated interaction with p97 could be negatively influenced.

## **5. Materials and Methods**

Standard experimental protocols as well as standard buffer solutions are not given in this section; please refer to *Molecular Cloning: A Laboratory Manual* (Sambrook, J., Fritsch, E.F., and Maniatis, T.; Cold Spring Harbor Laboratory Press, NY, Vols. 1-3 (1989)). Fine chemicals were from Sigma, unless indicated otherwise. Standard laboratory reagents were from local suppliers.

### **5.1. Mammalian Cell Culture**

#### *5.1.1. Culture conditions*

HEK293 cells (ATCC: CRL-1573), C2F3 cells (subclone of C2C12, Clemen et al., 1999; C2C12 ATCC: CRL-1772) and  $\Phi$ NX-E (S. Kinoshita and G. Nolan, Stanford University, USA) were grown in Dulbecco's modified Eagle's medium containing 4,5 g/l glucose (Sigma), supplemented with 10% fetal calf serum (FCS) (Biochrom), 2 mM L-glutamine (Biochrom), 1 mM sodium pyruvate (Biochrom), 100 U/ml penicillin G and 100  $\mu$ g/ml streptomycin (Invitrogen) in 5% CO<sub>2</sub> at 37°C. Differentiation of C2F3 myoblasts was induced replacing the FCS by 1% horse serum. Normal and IBMPFD primary human myoblasts were grown in skeletal muscle cell growth medium (Promocell, Germany; C-23060 with supplement mix C-39365 added).

### 5.1.2. *Transfection methods*

Transient transfection of HEK293 cells was carried out by electroporation ( $1 \times 10^6$  cells, 5  $\mu$ g plasmid; 475  $\mu$ F, 240 V, 4 mm cuvette). Stable HEK293 clones were obtained by selection with 1.2 mg/ml G418. Transient transfection of C2F3 cells using Lipofectamine was done according to the instructions of the manufacturer (Invitrogen, Germany). Transient co-transfection of pDsRed2-ER, pDsRed-Monomer-Golgi and pDsRed2-GAPDH in HEK293 cells stably overexpressing wt or mutant p97-GFP was carried out using FuGENE HD (Roche, Germany) according to the manufacturer's guidelines.

For transduction of C2F3 cells,  $\Phi$ NX-E cells were used to produce retrovirus particles.  $\Phi$ NX-E cells were seeded at  $2 \times 10^6$  cells in 60 mm dishes and transfected the next day using a calcium phosphate transfection protocol (Ausubel et al., 1998). 48 and 72 hours post transfection retroviral supernatant was collected, centrifuged to pellet cell debris, filtered through a 0,45  $\mu$ m filter and used for infection of target cells according to Springer and Blau (1997). Target C2F3 cells were seeded at  $1.5 \times 10^5$  per 60 mm dish at 24 hours prior to transduction. The distribution of the fusion protein was analyzed by indirect immunofluorescence and immunoblotting using antibodies directed against p97 and the FLAG epitope.

### 5.1.3. *Generation of growth curves*

Proliferation rates of stably transfected p97-GFP HEK293 cells, untransfected control HEK293 cells, and transduced and untransduced C2F3 cells were obtained by seeding cells at a density of  $1 \times 10^6$  cells / 60 mm dish in triplicate. After 24 h cells were trypsinized and counted again using a Neubauer counting chamber.

### 5.1.4. *Cell stress experiments*

To induce a stress response in cultured cells, various drugs and conditions were used. MG132 (Calbiochem, USA; 10 mM stock in DMSO; 5  $\mu$ M final concentration, 16h; Kitami et al., 2006; Weihl et al., 2006), Clasto-Lactacystin  $\beta$ -Lactone (Calbiochem; 10 mM stock in DMSO; 10  $\mu$ M final concentration, 24 h; Steinhilb and Gaut, 2001; Waelter et al. 2001), Wortmannin (Calbiochem, datasheet 681675; 1 mM stock in DMSO; 1  $\mu$ M final concentration, 22 h), H<sub>2</sub>O<sub>2</sub> (Sigma, Germany; 400  $\mu$ M final concentration, 16 h; Ardley et al. 2003) were added to the normal growth medium. Cells treated with MG132 were washed twice with PBS and further grown in fresh medium after 16 h of MG132 incubation. To cell cycle arrested cells (see cdk4 inhibitor below) MG132 was added with a delay of 6 h. For osmotic shock experiments, cells were incubated in 150 mM urea dissolved in normal culturing medium (Sigma, Germany; D'Alessandro et al., 2002) for 5 min. The solution was changed to fresh medium and cells were subsequently fixed after 4 min. UV-B irradiation experiments (total dose of 100 J/m<sup>2</sup> at a wavelength of 254 nm) were performed placing opened culture dishes containing a minimal volume of PBS in an UV-crosslinker (Hofer UVC 500, Amersham Pharmacia Biotech, Germany;

Westfall et al. 2005). Cells were further incubated in fresh medium and analyzed after 12 h. Mitomycin C treatment (medac, Germany; 10 µg/ml final concentration; standard protocol) was done for 3 h in normal culturing medium followed by two washing steps with PBS. Cells were subsequently analyzed after 1, 7 and 14 days. For continuous cell cycle arrest in G1 phase a CDK4 inhibitor (2-Bromo-12,13-dihydro-5H-indolo[2,3-a]pyrrolo[3,4-c]carbazole-5,7(6H)-dione; Calbiochem; 1 mM stock in DMSO; 200 nM final concentration; Zhu, G. et al., 2003) was added to the growth medium as indicated in the Results section. Cells were either fixated in 4% paraformaldehyde for microscopy or lysed in Laemmli buffer for Western blotting.

## **5.2. Imaging**

### *5.2.1. Indirect immunofluorescence and imaging of living cells*

Biopsies were fixed in 3% paraformaldehyde in a 0,2 M phosphate buffer, pH 7,4, for 2 h. After rinsing 5 times in 0,2 M phosphate buffer and PBS, the biopsies were infiltrated with saccharose at 12% and 18% to obtain a gradual substitution of saline solution with glucosate solution and then to avoid disruption of cellular membranes during successive phases. Finally, sections were frozen in liquid nitrogen.

Twenty-µm-thick sections were cut on a cryostat and collected on glass slides coated with 0,5% gelatin and 0,005% chromium potassium sulfate. To block nonspecific sites and to render the membranes permeable, sections were preincubated with 1% BSA and 0.3% Triton X-100 in PBS at room temperature for 15 min. Finally, sections were incubated with primary antibodies for 2 h. The first fluorochrome was

applied for 1 h after incubation with the primary antibody. For double-localization reactions, after 5 times rinsing with PBS and incubation with a biotinylated IgG in goat to obtain saturation of residual free binding sites, sections were incubated with a secondary antibody. Slides were finally washed in PBS and sealed with mounting medium.

Cells were seeded on coverslips and grown to approx. 50 – 70% confluency, washed with PBS and subsequently fixed either in -20°C methanol for 10 min or in 4% paraformaldehyde for 20 min followed by treatment with 0,5% Triton X-100 and PBS/Glycin 0,15% for 5 min each. Non-specific binding sites were blocked by incubating the cells twice for 15 min in PBG (0,5% BSA, 0,045% fish gelatine in PBS). Incubation with the primary antibody was performed at room temperature for 2 h. After 5 washes in PBS/Glycin, 5 min each, cells were incubated for 1 h with secondary antibody at room temperature, washed 5 times in PBS/Glycin and 4 times in PBS, 5 min each, rinsed in water and embedded in Gelvatol (Langanger et al., 1983).

Indirect immunofluorescence analysis as well as examination of living cells was done using a confocal laser scan microscope (Leica DM-IRBE; Leica, Germany).

### **5.2.2.     *Fluorescence protein protection (FPP) assay***

The fluorescence protein protection (FPP) assay was performed as described by Lorenz et al. (2006). Cells were fixed for microscopic analysis. Double transfected HEK293 cells (wt- or R155C-p97-GFP plus pDsRed2-ER, pDsRed-Monomer-Golgi or pDsRed2-GAPDH, respectively) were either directly fixed using 4% paraformaldehyde or first treated with 20 µM digitonin for 1 min followed by

4 mM trypsin for 5 min, both dissolved in KHM buffer (110 mM potassium acetate, 20 mM HEPES, 2 mM MgCl<sub>2</sub>)

### **5.3. Gel electrophoresis and Western blotting**

Gel electrophoresis and Western blotting of cultured cells were performed according to standard protocols (Sambrook, J., Fritsch, E.F., and Maniatis, T.; Cold Spring Harbor Laboratory Press, NY, Vols. 1-3 (1989))

For one- and two-dimensional gel electrophoresis, SDS-PAGE, protein transfer and visualization of muscle biopsies were carried out according to Clemen et al., 2005. 5 mg of human skeletal muscle specimen were pulverized by a pestle at  $-80^{\circ}\text{C}$ , suspended on ice in 200  $\mu\text{l}$  lysis buffer (80 mM HEPES–NaOH, pH 7.0, 1 mM PMSF, 1 mM EDTA, complete mini protease inhibitor(Roche)), homogenized 1 min by sonification on ice (Sonifier UP200S dr. hielscher) and centrifuged for 1 min at  $1000 \times g$ . 100  $\mu\text{l}$  of each sample were further centrifuged at  $125.000 \times g$  for 20 min at  $4^{\circ}\text{C}$ . The resulting pellet was resuspended in 200  $\mu\text{l}$  lysis buffer, sonificated and centrifuged again. The first supernatant and the remaining pellet of each sample were adjusted to equal volume with lysis buffer and used for 1D-SDS–PAGE and Western blotting analysis:

2D gel electrophoresis was performed according to Clemen et al., 2005 using an adaptation of the protocols described by Görg et al., Rabilloud et al. and the Amersham–Pharmacia Biotech protocol. 2 mg of each muscle specimen was cut at  $-80^{\circ}\text{C}$ , lysed in 200  $\mu\text{l}$  lysis buffer (7 M urea, 2 M thiourea, 4% CHAPS, 40 mM Tris, 2% IPG-buffer, 2% DTT, 1 mM PMSF, protease inhibitor (Roche), bromophenol blue) at room temperature, homogenized and centrifuged at  $16.000 \times g$

for 5 min. Samples of the supernatants were loaded with cups placed at the anodic and cathodic side of rehydrated 18 cm IPG-strips (pH 4–7 linear), focused at 22°C (Multiphor II horizontal) using the voltage gradient (power supply EPS 3501XL; 50 kVh) linearly increased on 400 V during 30 min, followed by 400 V for 4 h, linearly increased on 3500 V during 5 h, followed by 3500 V for 12.5 h. The strips were briefly rinsed in H<sub>2</sub>O and prepared for the second dimension by a two-step equilibration and cysteine alkylation process. The strips were incubated two times in equilibration buffer (Tris/HCl 50 mM, pH 8.8; 6 M Urea; 30% v/v glycerol; bromophenol blue) for 12 min, in which 4% (w/v) iodoacetamide was added. Subsequently, the strips were loaded on SDS gels (12.5% acrylamide) containing a small stacking gel according to Laemmli. Molecular weight standards were applied on a piece of filter paper positioned next to the basic end of the strip. Electrophoresis was carried out on a Hoefer SE 600 system at 20°C for which the current was limited to 25 mA per gel. Indirect immunoblotting was performed to standard protocols.

#### **5.4. p97-cDNA, site-directed mutagenesis and plasmids:**

Human wt-p97 cDNA was amplified by PCR, adding restriction sites, and a FLAG-tag at the 3' end. Therefore the following primers were used: hVCPfullExpF 5'-cggg atccaagcttcggccaccatggcttctggagccgattcaaaaggtgatgacctatcaa-3' and hVCPfullExpR 5'-atagtttagcggccgcaggtacctctttatcgtcatcgtctttgtagtcgccatacaggtcatcatcattgtcttctgtgtat acactgccacctgtgc-3'. For amplification of an N-terminal, 208 amino acids spanning cDNA, the following primers were used adding restriction sites, and a FLAG-tag at the 3' end: hVCPN208FLExpF 5'-cgggatccaagcttcggccaccatggcttctggagccgattcaaaa ggtgatgacc-3' and hVCPN208FLExpR 5'-atagtttagcggccgcaggtacctattatcgtcatcg

tctttgtagtcgccaccaatgtcatcataccctacttcattcaagg-3'. PCR-products were cloned in pGEMTeasy vector (Promega, Germany). The mutations R93C, R155H, and R155C were introduced using the site-directed mutagenesis kit (BD Biosciences, USA). The following primers were used: R93C-ivm 5'- cctaggcgtacgcaaaggttattcc-3', R155C-ivm 5'- catcccacc acagacaagaaaaatg-3', R155H-ivm: 5'- catcccaccatggacaagaaaaatg-3', and Select-ivm-rev: 5'- cgaagaacgatatccaatgatgagc-3' (changes an XmnI restriction site to EcoRV restriction site in the pGemTeasy vector for selection). Before further use plasmids were confirmed by restriction analysis and direct sequencing (Perkin-Elmer Cetus, USA). For transfection, the p97 cassettes were cloned into the pEGFP-N1 and pEGFP-C1 vectors (Clontech, USA). For viral transduction the cDNAs were cloned into the pBMN vector (pBMN-Z lacking the LacZ; S. Kinoshita and G. Nolan, Stanford University).

pDsRed2-ER and pDsRed-Monomer-Golgi were from Clontech (pDsRed2-ER vector No. 632409; pDsRed-Monomer-Golgi No. 632480; Clontech, USA). pDsRed2-GAPDH was obtained by cloning the GAPDH sequence from a GAPDH-CFP vector (GeneCopoeia, USA) C-terminally to DsRed2 into a pDsRed2 vector (Clontec, USA).

### **5.5. Generation of mouse targeting vector**

The homology arms of the targeting vector and the cDNA fragments to be used as southern probes have been amplified by PCR using BAC-clones RPCI23-124L1 and RPCI24-186I11 as templates. For the 5' southern probe, the following primers were used: VCPsou5F 5'-ggccagtttcctatgttg-3', VCPsou5R 5'-ggtggtcagtatct attaggtcta-3', VCPsou3F 5'-atatgccaccatgcccatctaaaag-3' and VCPsou3R 5'-cttgagtt



USA); monoclonal mouse anti-VCP/p97 (Affinity BioReagents, USA); monoclonal anti-VCP (BD Biosciences, USA); monoclonal mouse antibody raised against ubiquitin (Novocastra, UK); rabbit anti-ubiquitin polyclonal antibody (Stressgen, Canada); rabbit anti-ubiquitin polyclonal antibody (DAKO, Denmark); monoclonal mouse anti-poly-ubiquitin, clone FK2 (Stressgen, Canada); mouse monoclonal anti-desmin antibody D33 (DAKO, Denmark); rabbit polyclonal anti- $\alpha$ B-crystallin antiserum (Chemicon, USA); mouse monoclonal antibody raised against Ufd1 (Transduction Laboratories, USA); mouse monoclonal antibody raised against Ufd1 (BD Biosciences, USA), mouse monoclonal antibody raised against GST (Amersham Biosciences, Germany); mouse monoclonal anti-His antibody (Qiagen, Germany); mouse monoclonal anti-FLAG M2 antibody (Stratagene, USA); rabbit polyclonal enterokinase cleavage site (FLAG) antibody (Novus Biologicals, USA); TRITC-Phalloidin (Sigma, Germany); monoclonal mouse antibody specifically recognizing GFP (Noegel et al., 2004), monoclonal mouse anti-SCAP antibody (Santa Cruz, USA), polyclonal rabbit anti HMG CoA reductase antibody (upstate, USA). Isotype specific secondary antibodies conjugated with FITC, Cy3, or Texas Red, and Alexa568 were applied according to the recommendations of the manufacturers (Southern Biotechnology Associates, USA; Jackson ImmunoResearch Laboratories, USA; Molecular Probes, USA). Alternatively, sections incubated with anti-VCP and anti-ubiquitin antibodies were incubated with biotinylated secondary antibodies and the avidin-biotin complex. Visualization was performed with 3,3 diaminobenzidine or the APAP-complex as reagent.

## 5.8. Protein purification

*E. coli* strain BL21 expressing p97-GST constructs (wt, R93C, R155C or R155H) (kind gift of A. Böddrich after cloning our p97 cassettes into pGEX-6-P1-Vector) were grown in 250 ml LB-Medium at 37°C until  $OD_{600}=0,8$  followed by growing at RT till  $OD_{600}=1,0$ . Protein expression was induced by 0,1 mM IPTG and further incubating overnight at RT. Cells were centrifuged at 800 x g and washed once with TE-buffer. For cell lysis, the pellet was incubated with 10 ml lysis buffer (20 mM Tris-HCl pH 8,0, 100 mM NaCl, 2 mM EGTA, 2 mM Benzamidin, 4 mM DTT, 2 mM EDTA, 0,5 mM PMSF, 19 µg/ml Aprotinin, 10 µg/ml Leupeptin, 100 µg/ml Lysozym) for 15 min on ice and sonified for 3 min. After centrifugation at 20.000 x g for 30 min, the pellet was discarded and the supernatant incubated with 150 µl Glutathion-Beads (Sigma, Germany; equilibrated 2x in lysis buffer before adding) for 1 h at 4°C, washed 8x with 500 µl washing buffer (20 mM Tris-HCl pH 8,0 and 300 mM NaCl; centrifugation at 800 x g for 1 min), and finally incubated with 250 µl PreScission protease cleavage Puffer (50 mM Tris-HCl pH 7,5, 150 mM NaCl, 1 mM EDTA, 1 mM DTT). The PreScission protease (Roche, Germany) cleaves the GST-tag and itself can be removed by its GST-tag. 12 µl (24 U) of the protease were added to the beads for 2 h at 4°C. Cleaved p97 protein was eluted followed by an additional elution step with 200 µl cleavage buffer for 15 min. The eluted p97 protein was incubated with 50 µl of freshly equilibrated glutathion-beads for 1 h at 4°C to remove contamination with free GST. After centrifugation, the buffer was changed to PBS buffer. and finally the protein was concentrated using a Centricon (5.000 MWOC; Millipore, Germany). Protein concentrations were

determined using the Bradford assay (BioRad, Germany) and aliquots of 200 pmol protein were stored at -20°C until usage.

### **5.9. Filter assay**

Protein aliquots (p97 wt, R93C, R155C, R155H; 200 pmol each) were thawed on ice and centrifuged for 10 min at 16.000 x g. For negative control, BSA was used instead of the p97 protein. The potential ligands 16- $\alpha$ -Hydroxypregnenolone (Research Plus, USA) and 25-Hydroxycholesterol (Sigma, Germany) were dissolved in DMSO. 20 nmol were added to the protein (100x excess), and incubated at 22°C for 1 h. Samples were centrifuged at 5.000 x g at 4°C using Millipore Ultrafree-MC NMWL 10.000 Biomax 10 filters (Millipore, Germany). The flowthrough was kept for further analysis, the membrane bound protein-ligand complex was washed 4x with 160  $\mu$ l PBS supplemented with decreasing amounts of DMSO in each washing step (4,7%, 3%, 1,5%, 0%). To elute potentially bound ligands, the protein concentrate was incubated 2x for 5 min with 0,1% TFA in PBS and centrifuged. The flow through was kept for further analysis.

### **5.10. Proteasome assay**

Stably transfected HEK293 cells overexpressing wt-p97-FLAG-GFP and R155C-p97-FLAG-GFP and untransfected control cells were grown in 140 mm cell culture dishes up to approx. 80% confluence. Cell were trypsinized, counted using a Neubauer chamber, and adjusted to equal cell numbers. Cells were pelleted at 200 x g and lysed in 300  $\mu$ l homogenization buffer (50 mM Tris-HCl pH 7.2 ,1 mM

EDTA, 100 mM KCl, 5 mM MgCl<sub>2</sub>, 2 mM ATP, 0.04% (v/v) Nonidet P-40), sonified and centrifuged at 1.000 x g for 10 min followed by 16.000 x g for 15 min. To the latter supernatant 10% v/v glycerol was added. For storage, samples were snap frozen in liquid nitrogen and stored at -80°C. Protein concentrations were determined using a protein assay according to manufacturers protocol (BioRad, Germany). In addition, immunoblotting with an antibody directed against β-actin was performed. For each measurement of the proteasomal activity, 1,5 μg protein were added to a single well of a flat bottomed 96 well plate in reaction buffer (50 mM TrisHCl pH 8.0, 5 mM MgCl<sub>2</sub>, 5 mM ATP, 1 mM DTT) and adjusted to a total volume of 100 μl. Blank values were acquired by incubating 1,5 μg BSA instead of protein extracts. The peptides N-Suc-LLVY-7-amino-4-methylcoumarin- (AMC) (150 μM, chymotrypsin-like activity), Z-ARR-AMC (200 μM, trypsin-like activity) or Z-LLE-7-AMC (100 μM, caspase-like activity) (all Calbiochem, Germany), respectively, were added to test the indicated proteasome activities. To differentiate the proteasome activity from other peptidase activities the irreversible proteasome inhibitors Epoxomicin (1 μM; Calbiochem; inhibits chymotrypsin-like activity; Meng et al. 1999) and Adamantaneacetyl-(6-aminohexanoyl)3-(leucinyloxy)3-vinyl-(methyl)-sulfone (15 μM; Calbiochem; inhibits all three major peptidase activities; Kessler et al. 2001) were tested in a control experiment preincubating them with the proteasome extracts for 10 min at 37°C before adding the peptides. After incubation for 60, 70 and 80 min at 37°C, proteasomal activity was measured in a fluorescence microplate reader (Fluoroskan Ascent, Thermo Fisher Scientific, Germany) at 365 nm excitation and 460 nm emission.

**5.11. Statistical analysis**

Data are expressed as mean  $\pm$  standard deviation (SD). Statistical comparisons were made using Student's t-tests (unpaired, two-sided, unequal variance). A difference was considered significant at a value of  $p < 0.05$ .

## 6. References

- 1 Ardley, H. C., Scott, G. B., Rose, S. A., Tan, N. G., Markham, A. F. and Robinson, P. A. (2003) Inhibition of proteasomal activity causes inclusion formation in neuronal and non-neuronal cells overexpressing Parkin. *Mol Biol Cell*. 14, 4541-4556
- 2 Ausubel, F. M., Brent, R., Kingston, R.E., Moore, D.D., Seidman, J.G., Smith, J.A., and Struhl, K. (1998) *Current Protocols in Molecular Biology*., New York
- 3 Bakthavatsalam, D., Brazill, D., Gomer, R. H., Eichinger, L., Rivero, F. and Noegel, A. A. (2007) A G protein-coupled receptor with a lipid kinase domain is involved in cell-density sensing. *Curr Biol*. 17, 892-897
- 4 Bär, H., Fischer, D., Goudeau, B., Kley, R. A., Clemen, C. S., Vicart, P., Herrmann, H., Vorgerd, M. and Schröder, R. (2005) Pathogenic effects of a novel heterozygous R350P desmin mutation on the assembly of desmin intermediate filaments in vivo and in vitro. *Hum Mol Genet*. 14, 1251-1260
- 5 Bays, N. W., Wilhovsky, S. K., Goradia, A., Hodgkiss-Harlow, K. and Hampton, R. Y. (2001) HRD4/NPL4 is required for the proteasomal processing of ubiquitinated ER proteins. *Mol Biol Cell*. 12, 4114-4128
- 6 Bengoechea-Alonso, M. T. and Ericsson, J. (2007) SREBP in signal transduction: cholesterol metabolism and beyond. *Curr Opin Cell Biol*. 19, 215-222
- 7 Bledsoe, R. K., Montana, V. G., Stanley, T. B., Delves, C. J., Apolito, C. J., McKee, D. D., Consler, T. G., Parks, D. J., Stewart, E. L., Willson, T. M., Lambert, M. H., Moore, J. T., Pearce, K. H. and Xu, H. E. (2002) Crystal structure of the glucocorticoid receptor ligand binding domain reveals a novel mode of receptor dimerization and coactivator recognition. *Cell*. 110, 93-105

- 
- 8 Boeddrich, A., Gaumer, S., Haacke, A., Tzvetkov, N., Albrecht, M., Evert, B. O., Muller, E. C., Lurz, R., Breuer, P., Schugardt, N., Plassmann, S., Xu, K., Warrick, J. M., Suopanki, J., Wullner, U., Frank, R., Hartl, U. F., Bonini, N. M. and Wanker, E. E. (2006) An arginine/lysine-rich motif is crucial for VCP/p97-mediated modulation of ataxin-3 fibrillogenesis. *Embo J*
- 9 Bonifacino, J. S. and Weissman, A. M. (1998) Ubiquitin and the control of protein fate in the secretory and endocytic pathways. *Annu Rev Cell Dev Biol.* 14, 19-57
- 10 Braun, S., Matuschewski, K., Rape, M., Thoms, S. and Jentsch, S. (2002) Role of the ubiquitin-selective CDC48(UFD1/NPL4) chaperone (segregase) in ERAD of OLE1 and other substrates. *Embo J.* 21, 615-621
- 11 Brodsky, J. L. and Scott, C. M. (2007) Tipping the Delicate Balance: Defining How Proteasome Maturation Affects the Degradation of a Substrate for Autophagy and Endoplasmic Reticulum Associated Degradation (ERAD). *Autophagy.* 3
- 12 Burnett, B., Li, F. and Pittman, R. N. (2003) The polyglutamine neurodegenerative protein ataxin-3 binds polyubiquitylated proteins and has ubiquitin protease activity. *Hum Mol Genet.* 12, 3195-3205
- 13 Clemen, C. S., Fischer, D., Roth, U., Simon, S., Vicart, P., Kato, K., Kaminska, A. M., Vorgerd, M., Goldfarb, L. G., Eymard, B., Romero, N. B., Goudeau, B., Eggermann, T., Zerres, K., Noegel, A. A. and Schröder, R. (2005) Hsp27-2D-gel electrophoresis is a diagnostic tool to differentiate primary desminopathies from myofibrillar myopathies. *FEBS Lett.* 579, 3777-3782
- 14 Clemen, C. S., Hofmann, A., Zamparelli, C. and Noegel, A. A. (1999) Expression and localisation of annexin VII (synexin) isoforms in differentiating myoblasts. *J Muscle Res Cell Motil.* 20, 669-679
- 15 Confalonieri, F., Marsault, J. and Duguet, M. (1994) SAV, an archaeobacterial gene with extensive homology to a family of highly conserved eukaryotic ATPases. *J Mol Biol.* 235, 396-401

- 16 Dai, R. M. and Li, C. C. (2001) Valosin-containing protein is a multi-ubiquitin chain-targeting factor required in ubiquitin-proteasome degradation. *Nat Cell Biol.* 3, 740-744
- 17 D'Alessandro, M., Russell, D., Morley, S. M., Davies, A. M. and Lane, E. B. (2002) Keratin mutations of epidermolysis bullosa simplex alter the kinetics of stress response to osmotic shock. *J Cell Sci.* 115, 4341-4351
- 18 DeLaBarre, B. and Brunger, A. T. (2003) Complete structure of p97/valosin-containing protein reveals communication between nucleotide domains. *Nat Struct Biol.* 10, 856-863
- 19 Ding, W. X., Ni, H. M., Gao, W., Yoshimori, T., Stolz, D. B., Ron, D. and Yin, X. M. (2007) Linking of autophagy to ubiquitin-proteasome system is important for the regulation of endoplasmic reticulum stress and cell viability. *Am J Pathol.* 171, 513-524
- 20 Doss-Pepe, E. W., Stenroos, E. S., Johnson, W. G. and Madura, K. (2003) Ataxin-3 interactions with rad23 and valosin-containing protein and its associations with ubiquitin chains and the proteasome are consistent with a role in ubiquitin-mediated proteolysis. *Mol Cell Biol.* 23, 6469-6483
- 21 Edwards, P. A., Tabor, D., Kast, H. R. and Venkateswaran, A. (2000) Regulation of gene expression by SREBP and SCAP. *Biochim Biophys Acta.* 1529, 103-113
- 22 Eisenberg, I., Avidan, N., Potikha, T., Hochner, H., Chen, M., Olender, T., Barash, M., Shemesh, M., Sadeh, M., Grabov-Nardini, G., Shmilevich, I., Friedmann, A., Karpati, G., Bradley, W. G., Baumbach, L., Lancet, D., Asher, E. B., Beckmann, J. S., Argov, Z. and Mitrani-Rosenbaum, S. (2001) The UDP-N-acetylglucosamine 2-epimerase/N-acetylmannosamine kinase gene is mutated in recessive hereditary inclusion body myopathy. *Nat Genet.* 29, 83-87

- 23 Elkabetz, Y., Shapira, I., Rabinovich, E. and Bar-Nun, S. (2004) Distinct steps in dislocation of luminal endoplasmic reticulum-associated degradation substrates: roles of endoplasmic reticulum-bound p97/Cdc48p and proteasome. *J Biol Chem.* 279, 3980-3989
- 24 Fang, S., Ferrone, M., Yang, C., Jensen, J. P., Tiwari, S. and Weissman, A. M. (2001) The tumor autocrine motility factor receptor, gp78, is a ubiquitin protein ligase implicated in degradation from the endoplasmic reticulum. *Proc Natl Acad Sci U S A.* 98, 14422-14427
- 25 Feiler, H. S., Desprez, T., Santoni, V., Kronenberger, J., Caboche, M. and Traas, J. (1995) The higher plant *Arabidopsis thaliana* encodes a functional CDC48 homologue which is highly expressed in dividing and expanding cells. *Embo J.* 14, 5626-5637
- 26 Goldstein, J. L., DeBose-Boyd, R. A. and Brown, M. S. (2006) Protein sensors for membrane sterols. *Cell.* 124, 35-46
- 27 Gong, Y., Lee, J. N., Brown, M. S., Goldstein, J. L. and Ye, J. (2006) Juxtamembranous aspartic acid in Insig-1 and Insig-2 is required for cholesterol homeostasis. *Proc Natl Acad Sci U S A.* 103, 6154-6159
- 28 Gong, Y., Lee, J. N., Lee, P. C., Goldstein, J. L., Brown, M. S. and Ye, J. (2006) Sterol-regulated ubiquitination and degradation of Insig-1 creates a convergent mechanism for feedback control of cholesterol synthesis and uptake. *Cell Metab.* 3, 15-24
- 29 Halawani, D. and Latterich, M. (2006) p97: The cell's molecular purgatory? *Mol Cell.* 22, 713-717
- 30 Hampton, R. Y. (2002) ER-associated degradation in protein quality control and cellular regulation. *Curr Opin Cell Biol.* 14, 476-482
- 31 Hartmann-Petersen, R. and Gordon, C. (2004) Protein degradation: recognition of ubiquitylated substrates. *Curr Biol.* 14, R754-756

- 
- 32 Haubenberger, D., Bittner, R. E., Rauch-Shorny, S., Zimprich, F., Mannhalter, C., Wagner, L., Mineva, I., Vass, K., Auff, E. and Zimprich, A. (2005) Inclusion body myopathy and Paget disease is linked to a novel mutation in the VCP gene. *Neurology*. 65, 1304-1305
- 33 Hershko, A. and A., C. (1998) The ubiquitin system. *Annu Rev Biochem*. 67, 425-479.
- 34 Hetzer, M., Meyer, H. H., Walther, T. C., Bilbao-Cortes, D., Warren, G. and Mattaj, I. W. (2001) Distinct AAA-ATPase p97 complexes function in discrete steps of nuclear assembly. *Nat Cell Biol*. 3, 1086-1091
- 35 Hirabayashi, M., Inoue, K., Tanaka, K., Nakadate, K., Ohsawa, Y., Kamei, Y., Popiel, A. H., Sinohara, A., Iwamatsu, A., Kimura, Y., Uchiyama, Y., Hori, S. and Kakizuka, A. (2001) VCP/p97 in abnormal protein aggregates, cytoplasmic vacuoles, and cell death, phenotypes relevant to neurodegeneration. *Cell Death Differ*. 8, 977-984
- 36 Huang, Y., Niwa, J., Sobue, G. and Breitwieser, G. E. (2006) Calcium-sensing receptor ubiquitination and degradation mediated by the E3 ubiquitin ligase dorfins. *J Biol Chem*. 281, 11610-11617
- 37 Hübbers, C. U., Clemen, C. S., Kesper, K., Boddrich, A., Hofmann, A., Kamarainen, O., Tolksdorf, K., Stumpf, M., Reichelt, J., Roth, U., Krause, S., Watts, G., Kimonis, V., Wattjes, M. P., Reimann, J., Thal, D. R., Biermann, K., Evert, B. O., Lochmuller, H., Wanker, E. E., Schoser, B. G., Noegel, A. A. and Schroder, R. (2007) Pathological consequences of VCP mutations on human striated muscle. *Brain*. 130, 381-393
- 38 Ishigaki, S., Hishikawa, N., Niwa, J., Iemura, S., Natsume, T., Hori, S., Kakizuka, A., Tanaka, K. and Sobue, G. (2004) Physical and functional interaction between Dorfin and Valosin-containing protein that are colocalized in ubiquitylated inclusions in neurodegenerative disorders. *J Biol Chem*. 279, 51376-51385

- 39 Jarosch, E., Taxis, C., Volkwein, C., Bordallo, J., Finley, D., Wolf, D. H. and Sommer, T. (2002) Protein dislocation from the ER requires polyubiquitination and the AAA-ATPase Cdc48. *Nat Cell Biol.* 4, 134-139
- 40 Jentsch, S. and Rumpf, S. (2007) Cdc48 (p97): a "molecular gearbox" in the ubiquitin pathway? *Trends Biochem Sci.* 32, 6-11
- 41 Kayashima, T., Matsuo, H., Satoh, A., Ohta, T., Yoshiura, K., Matsumoto, N., Nakane, Y., Niikawa, N. and Kishino, T. (2002) Nonaka myopathy is caused by mutations in the UDP-N-acetylglucosamine-2-epimerase/N-acetylmannosamine kinase gene (GNE). *J Hum Genet.* 47, 77-79
- 42 Kessler, B. M., Tortorella, D., Altun, M., Kisselev, A. F., Fiebigler, E., Hekking, B. G., Ploegh, H. L. and Overkleeft, H. S. (2001) Extended peptide-based inhibitors efficiently target the proteasome and reveal overlapping specificities of the catalytic beta-subunits. *Chem Biol.* 8, 913-929
- 43 Kitami, M. I., Kitami, T., Nagahama, M., Tagaya, M., Hori, S., Kakizuka, A., Mizuno, Y. and Hattori, N. (2006) Dominant-negative effect of mutant valosin-containing protein in aggresome formation. *FEBS Lett.* 580, 474-478
- 44 Kobayashi, T., Manno, A. and Kakizuka, A. (2007) Involvement of valosin-containing protein (VCP)/p97 in the formation and clearance of abnormal protein aggregates. *Genes Cells.* 12, 889-901
- 45 Koegl, M., Hoppe, T., Schlenker, S., Ulrich, H. D., Mayer, T. U. and Jentsch, S. (1999) A novel ubiquitination factor, E4, is involved in multiubiquitin chain assembly. *Cell.* 96, 635-644
- 46 Kondo, H., Rabouille, C., Newman, R., Levine, T. P., Pappin, D., Freemont, P. and Warren, G. (1997) p47 is a cofactor for p97-mediated membrane fusion. *Nature.* 388, 75-78
- 47 Langanger, G., De Mey, J. and Adam, H. (1983) [1,4-Diazobicyclo-(2,2,2)-octane (DABCO) retards the fading of immunofluorescence preparations]. *Mikroskopie.* 40, 237-241

- 
- 48 Lass, A., McConnell, E., Nowis, D., Mechref, Y., Kang, P., Novotny, M. V. and Wojcik, C. (2007) A novel function of VCP (valosin-containing protein; p97) in the control of N-glycosylation of proteins in the endoplasmic reticulum. *Arch Biochem Biophys.* 462, 62-73
- 49 Lederkremer, G. Z. and Glickman, M. H. (2005) A window of opportunity: timing protein degradation by trimming of sugars and ubiquitins. *Trends Biochem Sci.* 30, 297-303
- 50 Lee, J. N., Song, B., DeBose-Boyd, R. A. and Ye, J. (2006) Sterol-regulated degradation of Insig-1 mediated by the membrane-bound ubiquitin ligase gp78. *J Biol Chem.* 281, 39308-39315
- 51 Levine, B. and Klionsky, D. (2004) Development by self-digestion: molecular mechanisms and biological functions of autophagy. *Dev Cell.* . Apr;6(4), 463-477
- 52 Li, Y., Suino, K., Daugherty, J. and Xu, H. E. (2005) Structural and biochemical mechanisms for the specificity of hormone binding and coactivator assembly by mineralocorticoid receptor. *Mol Cell.* 19, 367-380
- 53 Lilley, B. N. and Ploegh, H. L. (2005) Multiprotein complexes that link dislocation, ubiquitination, and extraction of misfolded proteins from the endoplasmic reticulum membrane. *Proc Natl Acad Sci U S A.* 102, 14296-14301
- 54 Lorenz, H., Hailey, D. W., Wunder, C. and Lippincott-Schwartz, J. (2006) The fluorescence protease protection (FPP) assay to determine protein localization and membrane topology. *Nat Protoc.* 1, 276-279
- 55 Lum, J., DeBerardinis, R. and Thompson, C. (2005) Autophagy in metazoans: cell survival in the land of plenty. *Nat Rev Mol Cell Biol.* Jun;6(6), 439-448
- 56 Matsumoto, M., Yada, M., Hatakeyama, S., Ishimoto, H., Tanimura, T., Tsuji, S., Kakizuka, A., Kitagawa, M. and Nakayama, K. I. (2004) Molecular clearance of ataxin-3 is regulated by a mammalian E4. *Embo J.* 23, 659-669

- 57 Medicherla, B., Kostova, Z., Schaefer, A. and Wolf, D. H. (2004) A genomic screen identifies Dsk2p and Rad23p as essential components of ER-associated degradation. *EMBO Rep.* 5, 692-697
- 58 Meng, L., Mohan, R., Kwok, B. H., Elofsson, M., Sin, N. and Crews, C. M. (1999) Epoxomicin, a potent and selective proteasome inhibitor, exhibits in vivo antiinflammatory activity. *Proc Natl Acad Sci U S A.* 96, 10403-10408
- 59 Meriin, A. B., Gabai, V. L., Yaglom, J., Shifrin, V. I. and Sherman, M. Y. (1998) Proteasome inhibitors activate stress kinases and induce Hsp72. Diverse effects on apoptosis. *J Biol Chem.* 273, 6373-6379
- 60 Meyer, H. H., Shorter, J. G., Seemann, J., Pappin, D. and Warren, G. (2000) A complex of mammalian ufd1 and npl4 links the AAA-ATPase, p97, to ubiquitin and nuclear transport pathways. *Embo J.* 19, 2181-2192
- 61 Meyer, H. H., Wang, Y. and Warren, G. (2002) Direct binding of ubiquitin conjugates by the mammalian p97 adaptor complexes, p47 and Ufd1-Npl4. *Embo J.* 21, 5645-5652
- 62 Mizuno, Y., Hori, S., Kakizuka, A. and Okamoto, K. (2003) Vacuole-creating protein in neurodegenerative diseases in humans. *Neurosci Lett.* 343, 77-80
- 63 Moir, D., Stewart, S. E., Osmond, B. C. and Botstein, D. (1982) Cold-sensitive cell-division-cycle mutants of yeast: isolation, properties, and pseudoreversion studies. *Genetics.* 100, 547-563
- 64 Nan, L., Wu, Y., Bardag-Gorce, F., Li, J., French, B. A., Wilson, L. T., Khanh Nguyen, S. and French, S. W. (2005) RNA interference of VCP/p97 increases Mallory body formation. *Exp Mol Pathol.* 78, 1-9
- 65 Nicholls, A., Bharadwaj, R. and Honig, B. (1993) GRASP: Graphical representation and analysis of surface properties. *Biophys J.* 64, A166
- 66 Noegel, A. A., Blau-Wasser, R., Sultana, H., Muller, R., Israel, L., Schleicher, M., Patel, H. and Weijer, C. J. (2004) The cyclase-associated protein CAP as regulator of cell polarity and cAMP signaling in *Dictyostelium*. *Mol Biol Cell.* 15, 934-945

- 
- 67 Pandey, U. B., Nie, Z., Batlevi, Y., McCray, B. A., Ritson, G. P., Nedelsky, N. B., Schwartz, S. L., DiProspero, N. A., Knight, M. A., Schuldiner, O., Padmanabhan, R., Hild, M., Berry, D. L., Garza, D., Hubbert, C. C., Yao, T. P., Baehrecke, E. H. and Taylor, J. P. (2007) HDAC6 rescues neurodegeneration and provides an essential link between autophagy and the UPS. *Nature*. 447, 859-863
- 68 Pinter, M., Jekely, G., Szepesi, R. J., Farkas, A., Theopold, U., Meyer, H. E., Lindholm, D., Nassel, D. R., Hultmark, D. and Friedrich, P. (1998) TER94, a *Drosophila* homolog of the membrane fusion protein CDC48/p97, is accumulated in nonproliferating cells: in the reproductive organs and in the brain of the imago. *Insect Biochem Mol Biol*. 28, 91-98
- 69 Rabinovich, E., Kerem, A., Frohlich, K. U., Diamant, N. and Bar-Nun, S. (2002) AAA-ATPase p97/Cdc48p, a cytosolic chaperone required for endoplasmic reticulum-associated protein degradation. *Mol Cell Biol*. 22, 626-634
- 70 Rabouille, C., Kondo, H., Newman, R., Hui, N., Freemont, P. and Warren, G. (1998) Syntaxin 5 is a common component of the NSF- and p97-mediated reassembly pathways of Golgi cisternae from mitotic Golgi fragments in vitro. *Cell*. 92, 603-610
- 71 Rape, M., Hoppe, T., Gorr, I., Kalocay, M., Richly, H. and Jentsch, S. (2001) Mobilization of processed, membrane-tethered SPT23 transcription factor by CDC48(UFD1/NPL4), a ubiquitin-selective chaperone. *Cell*. 107, 667-677
- 72 Ravikumar, B. and Rubinsztein, D. (2006) Role of autophagy in the clearance of mutant huntingtin: a step towards therapy? *Mol Aspects Med*. Oct-Dec;27(5-6), 520-527
- 73 Richly, H., Rape, M., Braun, S., Rumpf, S., Hoegel, C. and Jentsch, S. (2005) A series of ubiquitin binding factors connects CDC48/p97 to substrate multiubiquitylation and proteasomal targeting. *Cell*. 120, 73-84

- 
- 74 Rouiller, I., DeLaBarre, B., May, A. P., Weis, W. I., Brunger, A. T., Milligan, R. A. and Wilson-Kubalek, E. M. (2002) Conformational changes of the multifunction p97 AAA ATPase during its ATPase cycle. *Nat Struct Biol.* 9, 950-957
- 75 Rubinsztein, D. (2006) The roles of intracellular protein-degradation pathways in neurodegeneration. *Nature.* Oct 19, 443(7113), 780-786
- 76 Rubinsztein, D. C. (2007) Autophagy induction rescues toxicity mediated by proteasome inhibition. *Neuron.* 54, 854-856
- 77 Rumpf, S. and Jentsch, S. (2006) Functional division of substrate processing cofactors of the ubiquitin-selective Cdc48 chaperone. *Mol Cell.* 21, 261-269
- 78 Sambrook, J., Fritsch, E.F., and Maniatis, T. (1989) *Molecular cloning: a laboratory manual.* Cold Spring Harbor Laboratory Press, NY, Cold Spring Harbor
- 79 Schröder, R., Goudeau, B., Simon, M. C., Fischer, D., Eggermann, T., Clemen, C. S., Li, Z., Reimann, J., Xue, Z., Rudnik-Schoneborn, S., Zerres, K., van der Ven, P. F., Furst, D. O., Kunz, W. S. and Vicart, P. (2003) On noxious desmin: functional effects of a novel heterozygous desmin insertion mutation on the extrasarcomeric desmin cytoskeleton and mitochondria. *Hum Mol Genet.* 12, 657-669
- 80 Schröder, R., Watts, G. D., Mehta, S. G., Evert, B. O., Broich, P., Fliessbach, K., Pauls, K., Hans, V. H., Kimonis, V. and Thal, D. R. (2005) Mutant valosin-containing protein causes a novel type of frontotemporal dementia. *Ann Neurol.* 57, 457-461
- 81 Schuberth, C. and Buchberger, A. (2005) Membrane-bound Ubx2 recruits Cdc48 to ubiquitin ligases and their substrates to ensure efficient ER-associated protein degradation. *Nat Cell Biol.* 7, 999-1006
- 82 Schuberth, C., Richly, H., Rumpf, S. and Buchberger, A. (2004) Shp1 and Ubx2 are adaptors of Cdc48 involved in ubiquitin-dependent protein degradation. *EMBO Rep.* 5, 818-824

- 83 Selcen, D., Ohno, K. and Engel, A. G. (2004) Myofibrillar myopathy: clinical, morphological and genetic studies in 63 patients. *Brain*. 127, 439-451
- 84 Song, B. L., Javitt, N. B. and DeBose-Boyd, R. A. (2005) Insig-mediated degradation of HMG CoA reductase stimulated by lanosterol, an intermediate in the synthesis of cholesterol. *Cell Metab*. 1, 179-189
- 85 Song, B. L., Sever, N. and DeBose-Boyd, R. A. (2005) Gp78, a membrane-anchored ubiquitin ligase, associates with Insig-1 and couples sterol-regulated ubiquitination to degradation of HMG CoA reductase. *Mol Cell*. 19, 829-840
- 86 Spiro, R. G. (2002) Protein glycosylation: nature, distribution, enzymatic formation, and disease implications of glycopeptide bonds. *Glycobiology*. 12, 43R-56R
- 87 Springer, M. L. and Blau, H. M. (1997) High-efficiency retroviral infection of primary myoblasts. *Somat Cell Mol Genet*. 23, 203-209
- 88 Steinhilb, M. L., Turner, R. S. and Gaut, J. R. (2001) The protease inhibitor, MG132, blocks maturation of the amyloid precursor protein Swedish mutant preventing cleavage by beta-Secretase. *J Biol Chem*. 276, 4476-4484
- 89 Sun, L. P., Li, L., Goldstein, J. L. and Brown, M. S. (2005) Insig required for sterol-mediated inhibition of Scap/SREBP binding to COPII proteins in vitro. *J Biol Chem*. 280, 26483-26490
- 90 Tanenbaum, D. M., Wang, Y., Williams, S. P. and Sigler, P. B. (1998) Crystallographic comparison of the estrogen and progesterone receptor's ligand binding domains. *Proc Natl Acad Sci U S A*. 95, 5998-6003
- 91 Uchiyama, K., Jokitalo, E., Kano, F., Murata, M., Zhang, X., Canas, B., Newman, R., Rabouille, C., Pappin, D., Freemont, P. and Kondo, H. (2002) VCIP135, a novel essential factor for p97/p47-mediated membrane fusion, is required for Golgi and ER assembly in vivo. *J Cell Biol*. 159, 855-866
- 92 Uchiyama, K. and Kondo, H. (2005) p97/p47-Mediated biogenesis of Golgi and ER. *J Biochem (Tokyo)*. 137, 115-119

- 
- 93 Waelter, S., Boeddrich, A., Lurz, R., Scherzinger, E., Lueder, G., Lehrach, H. and Wanker, E. E. (2001) Accumulation of mutant huntingtin fragments in aggresome-like inclusion bodies as a result of insufficient protein degradation. *Mol Biol Cell*. 12, 1393-1407
- 94 Wang, Y., Satoh, A., Warren, G. and Meyer, H. H. (2004) VCIP135 acts as a deubiquitinating enzyme during p97-p47-mediated reassembly of mitotic Golgi fragments. *J Cell Biol*. 164, 973-978
- 95 Wanker, E. E., Scherzinger, E., Heiser, V., Sittler, A., Eickhoff, H. and Lehrach, H. (1999) Membrane filter assay for detection of amyloid-like polyglutamine-containing protein aggregates. *Methods Enzymol*. 309, 375-386
- 96 Watts, G. D., Wymer, J., Kovach, M. J., Mehta, S. G., Mumm, S., Darvish, D., Pestronk, A., Whyte, M. P. and Kimonis, V. E. (2004) Inclusion body myopathy associated with Paget disease of bone and frontotemporal dementia is caused by mutant valosin-containing protein. *Nat Genet*. 36, 377-381
- 97 Weihl, C. C., Dalal, S., Pestronk, A. and Hanson, P. I. (2006) Inclusion body myopathy-associated mutations in p97/VCP impair endoplasmic reticulum-associated degradation. *Hum Mol Genet*. 15, 189-199
- 98 Westfall, M. D., Joyner, A. S., Barbieri, C. E., Livingstone, M. and Pietenpol, J. A. (2005) Ultraviolet radiation induces phosphorylation and ubiquitin-mediated degradation of DeltaNp63alpha. *Cell Cycle*. 4, 710-716
- 99 Williams, S. P. and Sigler, P. B. (1998) Atomic structure of progesterone complexed with its receptor. *Nature*. 393, 392-396
- 100 Wu, S. Y., McNae, I., Kontopidis, G., McClue, S. J., McInnes, C., Stewart, K. J., Wang, S., Zheleva, D. I., Marriage, H., Lane, D. P., Taylor, P., Fischer, P. M. and Walkinshaw, M. D. (2003) Discovery of a novel family of CDK inhibitors with the program LIDAEUS: structural basis for ligand-induced disordering of the activation loop. *Structure*. 11, 399-410

- 
- 101 Ye, Y., Meyer, H. H. and Rapoport, T. A. (2001) The AAA ATPase Cdc48/p97 and its partners transport proteins from the ER into the cytosol. *Nature*. 414, 652-656
- 102 Ye, Y., Meyer, H. H. and Rapoport, T. A. (2003) Function of the p97-Ufd1-Npl4 complex in retrotranslocation from the ER to the cytosol: dual recognition of nonubiquitinated polypeptide segments and polyubiquitin chains. *J Cell Biol*. 162, 71-84
- 103 Ye, Y., Shibata, Y., Yun, C., Ron, D. and Rapoport, T. A. (2004) A membrane protein complex mediates retro-translocation from the ER lumen into the cytosol. *Nature*. 429, 841-847
- 104 Ye, Z. J., Kluger, Y., Lian, Z. and Weissman, S. M. (2005) Two types of precursor cells in a multipotential hematopoietic cell line. *Proc Natl Acad Sci U S A*. 102, 18461-18466
- 105 Yoshida, Y., Adachi, E., Fukiya, K., Iwai, K. and Tanaka, K. (2005) Glycoprotein-specific ubiquitin ligases recognize N-glycans in unfolded substrates. *EMBO Rep*. 6, 239-244
- 106 Zhang, S. H., Liu, J., Kobayashi, R. and Tonks, N. K. (1999) Identification of the cell cycle regulator VCP (p97/CDC48) as a substrate of the band 4.1-related protein-tyrosine phosphatase PTPH1. *J Biol Chem*. 274, 17806-17812
- 107 Zhang, X., Shaw, A., Bates, P., Newman, R., Gowen, B., Orlova, E., Gorman, M., Kondo, H., Dokurno, P., Lally, J., Leonard, G., Meyer, H., van Heel, M. and Freemont, P. (2000) Structure of the AAA ATPase p97. *Mol Cell*. , 1473-1484.
- 108 Zhong, X., Shen, Y., Ballar, P., Apostolou, A., Agami, R. and Fang, S. (2004) AAA ATPase p97/valosin-containing protein interacts with gp78, a ubiquitin ligase for endoplasmic reticulum-associated degradation. *J Biol Chem*. 279, 45676-45684

- 109 Zhu, G., Conner, S., Zhou, X., Shih, C., Brooks, H. B., Considine, E., Dempsey, J. A., Ogg, C., Patel, B., Schultz, R. M., Spencer, C. D., Teicher, B. and Watkins, S. A. (2003) Synthesis of quinolinyl/isoquinolinyl[a]pyrrolo [3,4-c] carbazoles as cyclin D1/CDK4 inhibitors. *Bioorg Med Chem Lett.* 13, 1231-1235

## 7. Abbreviations

BSA	Bovine serum albumine
CDC48	Cell division cycle protein 48
CDK4	Cyclin-dependent kinase 4
CHAPS	3-[(3-Cholamidopropyl)dimethylammonio]-1-propanesulfonate
DAPI	4',6-Diamidino-2-phenylindole
DMSO	Dimethyl sulfoxide
DTT	Dithiothreitol
EDTA	Ethylenediamine-tetraacetic acid
EGTA	Ethylene glycol-bis( $\beta$ -aminoethyl ether)-N,N,N',N'-tetraacetic acid
ER	Endoplasmic reticulum
ERAD	Endoplasmic reticulum associated protein degradation
FBS	Fetal bovine serum
FTD	Frontotemporal dementia
GAPDH	Glyceraldehyde-3-phosphate dehydrogenase
HEK	human embryonic kidney
HEPES	N-(2-Hydroxyethyl)piperazine-N'-(2-ethanesulfonic acid)
HMGR	HMG CoA reductase (3-hydroxy-3-methylglutaryl-coenzyme A reductase)
IBM	Inclusion body myopathy
IBMPFD	Inclusion body myopathy associated with Paget disease of the bone and frontotemporal dementia
Insig-1	Insulin-induced gene 1
IPTG	Isopropyl $\beta$ -D-1-thiogalactopyranoside
NP-40	Nonidet P-40
PAGE	Polyacrylamide gel electrophoresis
PBS	Phosphate buffered saline
PDB	Paget disease of the bone
PMSF	Phenylmethanesulfonyl fluoride
PMSF	Phenylmethylsulfonylfluorid
SCAP	SREBP-cleavage-activating protein
SDS	Sodium dodecyl sulfate
Sec24	Protein transport protein
SREBP	Sterol regulatory element-binding protein
TFA	Trifluoro acetic acid
Tris	Tris (hydroxymethyl) aminomethane / 2-Amino-2-(hydroxymethyl)-1,3-propanediol
Ufd1	Ubiquitin fusion degradation protein 1
VCP	Valosin containing protein

## 8. Abstract

Mutations in the p97 (VCP, valosin containing protein) gene cause a late-onset form of autosomal dominant Inclusion Body Myopathy associated with Paget disease of the bone and Frontotemporal Dementia (IBMPFD). p97 is an ubiquitously expressed member of the AAA-ATPase family with a tripartite structure comprising an N-terminal domain (Cdc48) involved in ubiquitin-binding, and two central D1- and D2-domains which hydrolyse ATP. p97 assembles into functional hexamers with a central cylinder formed by the D-domains surrounded by the N-domains. p97 has been associated with a wide variety of essential cellular processes including the ubiquitin proteasome protein degradation system and along with its cofactors Ufd1, Npl4, and Derlin-1 with the endoplasmic reticulum associated protein degradation (ERAD).

In this work the pathological consequences of three heterozygous p97-mutations (R93C, R155H, R155C; located in the N-terminal Cdc48 domain of the p97 protein) on human striated muscle *in vivo* and *in vitro* are presented. IBMPFD skeletal muscle pathology is characterized by degenerative changes and filamentous p97- and ubiquitin-positive cytoplasmic and nuclear protein aggregates. Furthermore, mutant p97 leads to a novel form of dilatative cardiomyopathy with inclusion bodies.

Pull-down experiments showed that all three p97 mutations do not affect the binding to Ufd1, Npl4, and ataxin-3. Structural analysis demonstrated that R93 and R155 are both surface-accessible residues located in the center of cavities that may enable ligand binding. The search for putative ligands to the R93 and R155 cavities resulted in the identification of cyclic sugar compounds and a sterol-like compound providing a novel link to p97 carbohydrate and sterol interactions in the complex pathology of IBMPFD. Analysis of stably transfected HEK293 cells showed a significantly decreased proteasome activity for cells overexpressing mutated R155C-p97 and a prominent upregulation of its autophagic activity. The R155C-p97 overexpressing HEK293 cells also showed a significant delay in clearing aggregates induced by proteasome inhibition. Immunoblotting of cell lysates derived from proteasome inhibited HEK293 cells and after the reactivation of its proteasomal activity pointed to a missregulation of the cholesterol homeostasis pathway in HEK293 cells overexpressing mutated R155C-p97 indicating a disrupted ERAD function caused by R155C mutated p97.

## 9. Zusammenfassung

Mutationen im p97 (VCP, valosin containing protein) Gen verursachen eine spät auftretende Form einer autosomal dominanten Einschlusskörper-Myopathie assoziiert mit der Paget-Erkrankung der Knochen und einer frontotemporalen Demenz (IBMPFD). p97 ist ein ubiquitinär exprimierter Vertreter der AAA-ATPase-Familie mit einer dreiteiligen Struktur bestehend aus einer N-terminalen Domäne (Cdc48), welche in die Ubiquitin-Bindung involviert ist, und zwei zentralen D1- und D2-Domänen, welche ATP hydrolisieren. p97 lagert sich zu einem funktionalen Homohexamer zusammen, bestehend aus einem aus den D-Domänen gebildeten zentralen Zylinder, welcher von den N-Domänen umgeben wird. p97 wurde mit einer Vielzahl von essenziellen zellulären Prozessen in Verbindung gebracht, darunter das Ubiquitin-Proteasom-Degradationssystem und einschließlich seiner Co-Faktoren Ufd1, Npl4 und Derlin-1 mit dem Endoplasmatischen Retikulum assoziierten Degradationssystem (ERAD).

In dieser Arbeit wurden die pathologischen Konsequenzen von drei heterozygoten p97-Mutationen (R93C, R155H und R155C; alle lokalisiert in der N-terminalen Cdc48-Domäne des p97 Proteins) anhand menschlicher quergestreifter Muskulatur *in vivo* und *in vitro* analysiert. Charakteristisch für die IBMPFD-Skelettmuskelpathologie sind degenerative Veränderungen und filamentöse p97- und Ubiquitin-positive cytoplasmatische und nukleäre Proteinaggregate. Außerdem führt mutiertes p97 zu einer neuen Form der dilatativen Kardiomyopathie mit Einschlusskörperchen.

Pull-down Experimente konnten zeigen, dass alle drei p97-Mutationen keinen Effekt auf die Bindung mit Ufd1, Npl4 und Ataxin-3 haben. Strukturuntersuchungen zeigten, dass die Aminosäuren R93 und R155 frei zugänglich an der Oberfläche von p97 liegen. Beide bilden die Zentren von potentiellen Bindetaschen und könnten eine Ligandenbindung ermöglichen. Die Suche nach potentiellen Liganden für die R93 und R155 Bindetaschen ergab verschiedene zyklische Zuckerverbindungen und ein Sterol. Diese Ergebnisse eröffnen eine neue Verbindung zwischen p97 und einer Karbohydrat- und Sterol-Interaktion in der komplexen Pathologie der IBMPFD-Erkrankung. Stabil transfizierte HEK239-Zellen zeigten eine signifikante Abnahme der Proteasom-Aktivität in R155C-p97 überexprimierenden Zellen und eine deutliche Zunahme von deren Autophagie-Aktivität. Außerdem zeigten diese R155C-p97 überexprimierenden HEK293-Zellen eine deutlich verzögerte Abbauaktivität von per Proteasominhibition induzierten Proteinaggregaten. Immunoblots von Zelllysaten aus Proteasom-inhibierten HEK293-Zellen und nach anschließender Proteasomreaktivierung wiesen auf eine Fehlregulation des Cholesteroll-Homöostase-Signalweges für R155C-p97 überexprimierende Zellen hin. Dies impliziert eine gestörte ERAD-Funktion, verursacht durch die R155C-p97-Mutation.

## 10. Erklärung

Ich versichere, dass ich die von mir vorgelegte Dissertation selbständig angefertigt, die benutzten Quellen und Hilfsmittel vollständig angegeben und die Stellen der Arbeit- einschließlich Tabellen und Abbildungen-, die anderen Werken im Wortlaut oder dem Sinn nach entnommen sind, in jedem Einzelfall als Entlehnung kenntlich gemacht habe; dass diese Dissertation noch keiner anderen Fakultät oder Universität zur Prüfung vorgelegen hat; dass sie - abgesehen von unten angegebenen Teilpublikationen noch nicht veröffentlicht ist, sowie, dass ich eine Veröffentlichung vor Abschluss des Promotionsverfahrens nicht vornehmen werde. Die Bestimmungen dieser Promotionsordnung sind mir bekannt. Die von mir vorgelegte Dissertation ist von Frau Prof. Dr. Angelika A. Noegel und Herrn Dr. Christoph S. Clemen betreut worden.

Köln, den 03.10.2007

Christian U. Hübbers

Teilpublikation:

Hübbers CU, Clemen CS, Kesper K, Böddrich A, Hofmann A, Kämäräinen O, Tolksdorf K, Stumpf M, Reichelt J, Roth U, Krause S, Watts G, Kimonis V, Wattjes MP, Reimann J, Thal DR, Biermann K, Evert BO, Lochmüller H, Wanker EE, Schoser BG, Noegel AA, Schröder R. Pathological consequences of VCP mutations on human striated muscle. *Brain*. 2007 Feb;130(Pt 2):381-93.

## 11. Curriculum vitae / Lebenslauf

### ZUR PERSON

Name	Christian Ulrich Hübbers
Anschrift	Blumentalstr. 35 42859 Remscheid
Geburtsdatum	22.01.1975 in Köln
Familienstand	Verheiratet, keine Kinder
Staatsangehörigkeit	Deutsch

### AUSBILDUNG

11/04 – 11/07	<b>Promotion in Biochemie</b> bei Frau Prof. Dr. Angelika A. Noegel, Institut für Biochemie I der medizinischen Fakultät der Universität zu Köln
06/03 - 07/04	<b>Diplomarbeit, Abschluss: Diplom Biologe</b> Diplomarbeit bei Herrn Prof. Dr. Stefan Berking, I. Zoologisches Institut der Universität zu Köln, Abteilung Experimentelle Morphologie Thema: Untersuchungen zu Genregulatoren und ihrer Expression an Hydrozoen
WS 98 – SS 03	Diplomstudiengang Biologie an der Universität zu Köln
SS 96 - SS 98	Diplomstudiengang Chemie an der Universität zu Köln
10/94 - 12/95	Zivildienst bei der Johanniter-Unfall-Hilfe Köln
1985 - 1994	Elisabeth von Thüringen Gymnasium, Köln Abschluss: Abitur
1981 – 1985	Katholische Grundschule Berrenrather Str., Köln